



# Impacts of early autumn Arctic sea ice concentration on subsequent spring Eurasian surface air temperature variations

Shangfeng Chen<sup>1</sup> · Renguang Wu<sup>1,2</sup>

Received: 19 May 2017 / Accepted: 26 November 2017 / Published online: 30 November 2017  
© Springer-Verlag GmbH Germany, part of Springer Nature 2017

## Abstract

This study reveals a close relation between autumn Arctic sea ice change (SIC) in the Laptev Sea-eastern Siberian Sea-Beaufort Sea and subsequent spring Eurasian surface air temperature (SAT) variation. Specifically, more (less) SIC over the above regions in early autumn generally correspond to SAT warming (cooling) over the mid-high latitudes of Eurasia during subsequent spring. Early autumn Arctic SIC affects spring Eurasian SAT via modulating spring Arctic Oscillation (AO) associated atmospheric changes. The meridional temperature gradient over the mid-high latitudes decreases following the Arctic sea ice loss. This results in deceleration of prevailing westerly winds over the mid-latitudes of the troposphere, which leads to increase in the upward propagation of planetary waves and associated Eliassen-Palm flux convergence in the stratosphere over the mid-high latitudes. Thereby, westerly winds in the stratosphere are reduced and the polar vortex is weakened. Through the wave-mean flow interaction and downward propagation of zonal wind anomalies, a negative spring AO pattern is formed in the troposphere, which favors SAT cooling over Eurasia. The observed autumn Arctic SIC-spring Eurasian SAT connection is reproduced in the historical simulation (1850–2005) of the flexible global ocean-atmosphere-land system model, spectral version 2 (FGOALS-s2). The FGOALS-s2 also simulates the close connection between autumn SIC and subsequent spring AO. Further analysis suggests that the prediction skill of the spring Eurasian SAT was enhanced when taking the autumn Arctic SIC signal into account.

**Keywords** Autumn Arctic sea ice · Surface air temperature · Spring Arctic Oscillation

## 1 Introduction

Variations in surface air temperature (SAT) have pronounced impacts on agriculture, socioeconomic development, and people's daily lives. For example, low summer SAT over Northeast China may lead to a significant reduction in local crop yield (Sun et al. 1983; Yao 1995). Soil moisture change

induced by the SAT variation may influence surface water characteristics and water and energy exchange between the land and the lower atmosphere (e.g., Henderson-Sellers 1996). The broad wildfires and the large economic loss over Europe in summer of 2003 were related to the extremely high SAT (e.g., Beniston 2004; Stott et al. 2004). Therefore, it is important to investigate the factors for the SAT variability.

The interannual variations in SAT over Eurasia are impacted by various factors, including the North Atlantic Oscillation (NAO) (Hurrell and van Loon 1997; Sun et al. 2008; Zveryaev and Gulev 2009; Ionita et al. 2012), the Arctic Oscillation (AO) (Thompson and Wallace 1998; Miyazaki and Yasunari 2008; Kim and Ahn 2012; Cheung et al. 2012; Chen et al. 2013), the North Atlantic sea surface temperature (SST) variation (Wu et al. 2011a; Chen et al. 2016a), the El Niño-Southern Oscillation (ENSO) (Wu et al. 2010; Graf and Zanchettin 2012), and the Eurasian snow cover (Wu et al. 2014; Ye et al. 2015; Wu and Chen 2016; Chen et al. 2016a). For instance, large parts of Eurasian

---

**Electronic supplementary material** The online version of this article (<https://doi.org/10.1007/s00382-017-4026-x>) contains supplementary material, which is available to authorized users.

✉ Renguang Wu  
renguang@mail.iap.ac.cn

<sup>1</sup> Center for Monsoon System Research, Institute of Atmospheric Physics, Chinese Academy of Sciences, Beijing 100029, China

<sup>2</sup> State Key Laboratory of Numerical Modeling for Atmospheric Sciences and Geophysical Fluid Dynamics, Institute of Atmospheric Physics, Chinese Academy of Sciences, Beijing, China

continent are covered by positive (negative) SAT anomalies during winter when the NAO or AO is in its positive (negative) phase (Gong et al. 2001; Wu and Wang 2002). The North Atlantic SST anomalies induce an atmospheric teleconnection pattern extending from the North Atlantic eastward to Eurasia and affect the Eurasian spring SAT via wind-induced temperature advection (Ye et al. 2015; Chen et al. 2016a). Chen et al. (2016a) indicated that local snow cover changes contribute to spring SAT variation in some regions of Eurasia via modulating surface shortwave radiation.

Arctic sea ice is an important component of the Earth's climate system and it plays a crucial role in the surface energy exchange between the lower atmosphere and ocean (Serreze et al. 2007). The rapid Arctic warming and enhancement of the precipitation over the Arctic during recent decades may be related to decline in the Arctic sea ice (e.g., Deser et al. 2010; Screen and Simmonds 2010). During recent decades, increasing attention were paid to the possible linkage between the Arctic sea ice variation and climate change over the mid-high latitudes of the Northern Hemisphere (NH), especially Eurasia (e.g., Wu et al. 2011b, 2016; Inoue et al. 2012; Li and Wu 2012; Li and Wang 2013; Vihma 2014; Nakamura et al. 2015; Gao et al. 2015). Several studies indicated that the frequent extremely cold winter and snow storm over Eurasia during recent decades (such as 2009/10) may be attributed to the Arctic sea ice loss (Petoukhov and Semenov 2010; Francis and Vavrus 2012; Liu et al. 2012a, b; Tang et al. 2013). Chen et al. (2014b) and Sun et al. (2016b) showed that the East Asian winter monsoon and associated SAT anomalies were significantly influenced by preceding autumn Arctic sea ice. Zuo et al. (2016) reported that autumn Arctic sea ice change has a large influence on winter SAT in China via modulating the Siberian High. Note that the current climate models have considerable uncertainties in reproducing the connection between the Arctic sea ice change and the Eurasian climate anomalies (e.g., Honda et al. 2009; Liu et al. 2012a, b; Kug et al. 2015; McCusker et al. 2016; Sun et al. 2016a).

Previous studies are mostly concerned with the impacts of the Arctic sea ice changes on winter SAT. It is unclear whether changes in the preceding Arctic sea ice may affect subsequent spring Eurasian SAT variations. In this study, we present evidences to show that spring SAT variations over the mid-high latitudes of Eurasia were significantly connected with the changes in the preceding autumn Arctic sea ice. Note that spring Eurasian SAT variations may play an important role in connecting the preceding winter atmospheric anomalies and the subsequent summer climate and the Asian summer monsoon activity (e.g., Ogi et al. 2003). Variations in spring SAT over the Eurasian continent may modulate the Asian summer monsoon through changing the temperature differences between the continent and the

surrounding oceans (e.g., Liu and Yanai 2001; D'Arrigo et al. 2006). In addition, boreal spring is the time when most of the climate models suffer the well known "predictability barrier" related to the ENSO (Webster and Yang 1992) that decreases the prediction skill of the dynamical models. Hence, it is important to identify other sources of predictability for the Eurasian spring SAT variability.

We analyze the physical processes responsible for the influence of early autumn Arctic sea ice on the subsequent spring Eurasian SAT variations. The rest of the present study is arranged as follows. Section 2 describes the datasets and methods used in this study. Section 3 presents observational evidences for the connection between early autumn Arctic sea ice and subsequent spring Eurasian SAT variations. Section 4 discusses the plausible physical mechanism for the impact of early autumn Arctic sea ice on the following spring Eurasian SAT. Section 5 examines reproducibility of the autumn Arctic SIC-spring SAT connection in the historical simulation of a fully coupled global climate model. Section 6 develops an empirical model of spring Eurasian SAT based on preceding Arctic sea ice variation. Section 7 gives a summary and discussion.

## 2 Data and methods

Monthly mean SAT used in this study is provided by the University of Delaware (Matsuura and Willmott 2009). This SAT dataset has a regular  $0.5^\circ$  latitude-longitude grid and is available from 1900 to 2014. Monthly mean sea ice concentration (SIC) data are extracted from the Hadley Centre Sea Ice and Sea Surface Temperature dataset (HadISST) since 1870 with a horizontal resolution of  $1^\circ \times 1^\circ$  (Rayner et al. 2003; <http://www.metoffice.gov.uk/hadobs/hadisst>). We also use the SIC data provided by the National Snow and Ice Data Center (NSIDC) (Peng et al. 2013; <http://nsidc.org/data>) to confirm the results derived from the HadISST. The NSIDC SIC data are provided in the polar stereographic projection on a  $25 \times 25$  km grid, which are available from October 1978 to May 2015. Note that the raw NSIDC SIC data have been converted to a regular  $1^\circ \times 1^\circ$  horizontal grid for this analysis. The results obtained in this study based on NSIDC SIC data are very similar to those based on HadISST SIC data. Hence, we only display the results derived from the HadISST SIC unless otherwise stated. Results based on the NSIDC SIC data are provided in the supplementary material.

The present study employs monthly and daily mean sea level pressure (SLP), geopotential height, air temperature, winds from the ERA-Interim dataset from 1979 to the present (Dee et al. 2011; <http://apps.ecmwf.int/datasets/>). The daily mean data are employed to calculate the Eliassen-Palm (EP) flux, as described below. The ERA-Interim dataset has a horizontal resolution of  $1.5^\circ \times 1.5^\circ$  and extends from

1000-hPa to 1-hPa. The time period of the present analysis is from 1979 to 2014 during which all the variables are available. This study focuses on the variations on the interannual timescales. All the variables are subjected to a 7 year high pass Lanczos filter (Duchon 1979) to obtain the component of interannual variations. The statistical significances of the correlation coefficient and anomalies based on regression are estimated according to the two-tailed Student's  $t$  test.

We employ the EP flux to detect the quasi-stationary planetary wave propagation (Edmon et al. 1980; Plumb 1985). The EP flux components ( $\bar{F}$ ) and its divergence ( $D_F$ ) are shown as follows:

$$F_\varphi = -\rho r \cos \varphi \overline{u'v'}$$

$$F_p = -\rho r \cos \varphi \frac{Rf}{HN^2} \overline{v'T'}$$

$$D_F = \frac{\nabla \cdot \bar{F}}{\rho r \cos \varphi}$$

Here,  $\rho$ ,  $\varphi$ ,  $r$ ,  $R$ , and  $f$  represent the air density, the latitude, the radius of the earth, the gas constant, and the Coriolis parameter, respectively.  $H$  is the scale height, and  $N$  denotes the buoyancy frequency. Note that  $N$  is calculated from the temperature data.  $u$ ,  $v$ , and  $T$  are zonal and meridional wind, and temperature, respectively. Overbars denote zonal average, and primes denote zonal deviation. Via expanding geopotential height into zonal Fourier harmonics, zonal wavenumbers 1–3 are generally employed to represent quasi-stationary planetary wave activity. Based on previous studies (Plumb 1985; Chen et al. 2003), the EP flux divergence is a good diagnostic tool to detect the forcing of the eddy to zonal mean flow. In particular, divergence (convergence) of EP flux results in the acceleration (deceleration) of westerly winds (Chen et al. 2002, 2003; Vallis 2006).

### 3 Connection between spring Eurasian SAT and preceding autumn Arctic SIC

An empirical orthogonal function (EOF) analysis was performed to obtain the leading mode of spring (March–April-averaged) SAT variations over the mid-high latitudes of Eurasia (40°–70° N and 0°–140° E) during 1979–2014. Following North et al. (1982a), SAT anomalies are weighted by cosine of the latitude in the EOF analysis to account for the decrease of area towards the North Pole. Figure 1 displays the first EOF (EOF1) mode and the corresponding principal component time series (PC1) of the spring Eurasian SAT interannual variations. EOF1 explains 43.9% of the total variance and is well separated from the other modes according to the method of North et al. (1982b). The EOF1

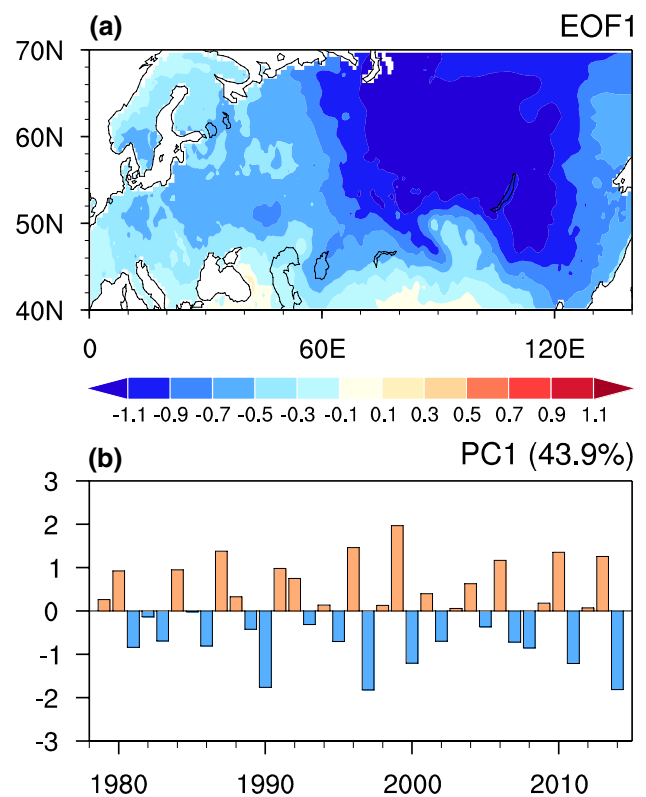


**Fig. 1** **a** The first EOF (EOF1) mode of interannual variation of spring [March–April, MA(0)] surface air temperature (SAT) anomalies over the mid-high latitudes of Eurasia. **b** The corresponding PC1 time series of the first EOF mode

is featured by same-sign SAT anomalies over the mid-high latitude Eurasian continent, with the largest loading over Siberia (Fig. 1a). The corresponding PC time series displays obvious year-to-year variations (Fig. 1b).

Before analyzing the possible link between Arctic SIC and spring Eurasian SAT variations, we first display spring atmospheric circulation anomalies related to the first EOF mode of spring Eurasian SAT. Figure 2 shows spring SLP, 850-hPa winds, 500 and 200-hPa geopotential height anomalies obtained by regression on the normalized PC1 of spring Eurasian SAT. The distributions of pressure, wind, and height anomalies in Fig. 2 bear a close resemblance to those in the negative phase of spring AO (Chen et al. 2014a, 2016a). The correlation coefficient between PC1 of spring Eurasian SAT and spring AO index is 0.78, significant at the 99% confidence level based on the Student's  $t$  test. Here, spring AO index is defined as the PC time series corresponding to the EOF1 of spring SLP anomalies north of 20°N.

Corresponding to positive PC1, pronounced positive SLP anomalies occur over the polar region and northern Eurasia, and significant negative SLP anomalies appear over the east coast of Europe and southeastern China (Fig. 2a). At 850-hPa, a significant anomalous cyclone is observed over

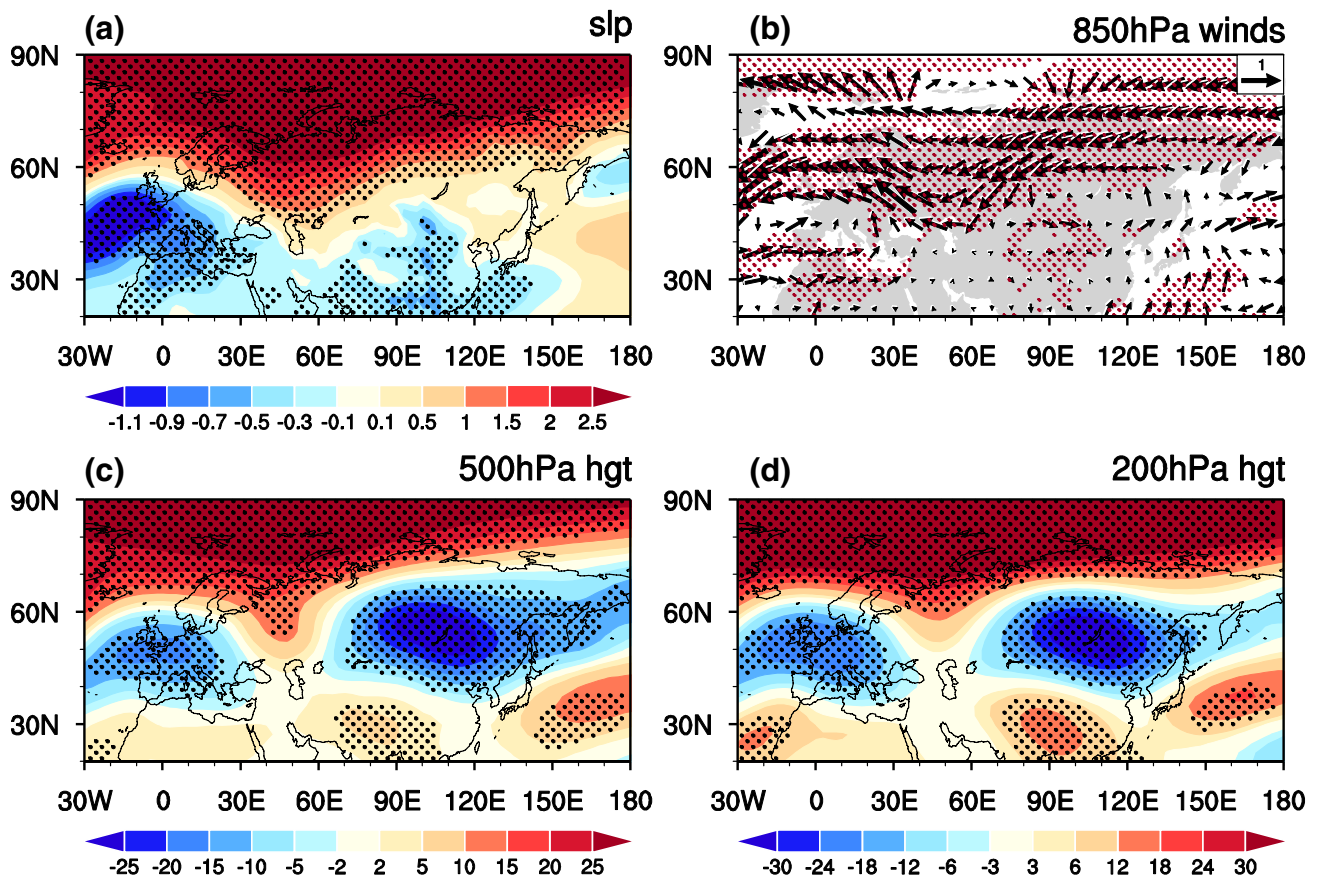


**Fig. 2** Anomalies of spring **a** SLP (unit: hPa), **b** 850-hPa winds (unit:  $\text{m s}^{-1}$ ), **c** 500-hPa and **d** 200-hPa geopotential height (unit: gpm) regressed upon the normalized PC1 of spring Eurasian SAT. Stippling in **a**, **c**, **d** indicates anomalies that significantly different from

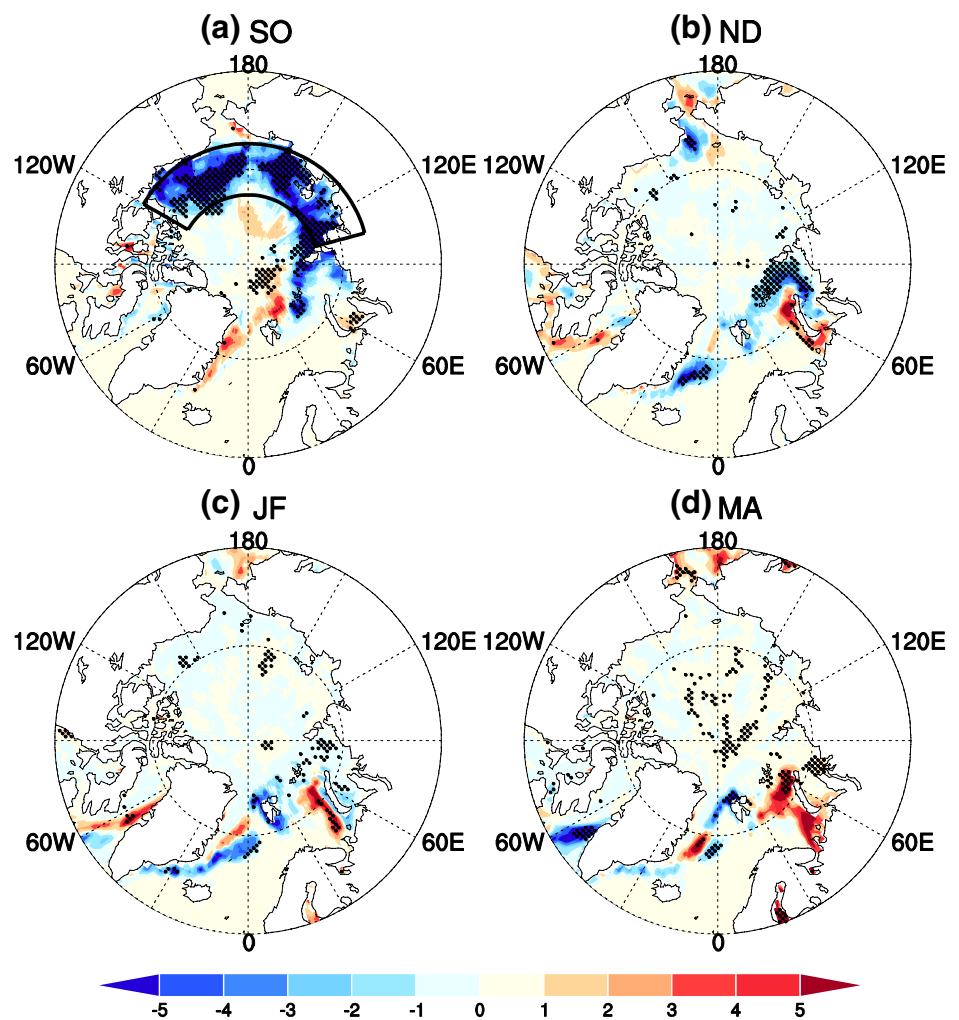
zero at the 95% confidence level. Stippling in **(b)** indicates regions where either component of the wind anomalies is significantly different from zero at the 95% confidence level according to the Student's  $t$  test

east Europe and northeast Asia, and a marked anomalous anticyclone is present over the Eurasian part of the Arctic (Fig. 2b). Consequently, there are pronounced northeasterly wind anomalies over most parts of the mid-high latitude Eurasian continent (Fig. 2b). These anomalous northeasterly winds explain the formation of negative SAT anomalies over the mid-high latitudes of Eurasia mainly via wind-induced temperature advection (Ye et al. 2015; Chen et al. 2016a). Geopotential height anomalies in the mid-upper troposphere (500 and 200-hPa) display an equivalent barotropic structure, with significant positive anomalies over the Arctic region and subtropics and negative anomalies over the mid-latitudes of Eurasia (Fig. 2c, d). Note that two centers of significant negative geopotential height anomalies are observed over east Europe and northeast Asia (Fig. 2c, d), respectively, corresponding well with anomalous cyclones there (Fig. 2b).

To examine whether there exists a connection between preceding Arctic SIC variation and the spring Eurasian SAT change, we first calculated the Arctic SIC anomalies in association with the EOF1 of spring Eurasian SAT.

Figure 3 shows Arctic SIC anomalies at September–October (SO)(– 1), November–December (ND)(– 1), January–February (JF)(0), and March–April (MA)(0) obtained by regression on the normalized PC1 of spring Eurasian SAT. SIC data in constructing Fig. 3 were derived from the HadISST dataset. Results are very similar when using the SIC data from the NSIDC (Figure S1 in the supporting material). In this study, the time notations (– 1) and (0) refer to the year before and during the spring Eurasian SAT year, respectively. At SO(– 1), significant and negative SIC anomalies extend from the Laptev Sea and eastern Siberian Sea to the Beaufort Sea (Fig. 3a). At ND(– 1), JF(0), and MA(0), significant Arctic SIC anomalies cover small regions in the Barents Sea, the Kara Sea, the Greenland Sea, or the Labrador Sea (Fig. 3b–d). Above results indicate that spring SAT anomalies over the mid-high latitudes of Eurasia have a close connection with SIC anomalies in preceding early autumn [SO(– 1)] in the Laptev-eastern Siberian-Beaufort seas. When there is more (less) SIC over the above mentioned regions in preceding

**Fig. 3** Anomalies of Arctic sea ice concentration (SIC) (unit: %) in preceding SO(-1), ND(-1), JF(0), and MA(0) regressed upon the normalized PC1 of spring [MA(0)] Eurasian SAT. Stippling regions indicate anomalies that significantly different from zero at the 95% confidence level. SIC data were derived from the HadISST



early autumn, the following spring SAT tends to be higher (lower) over the mid-high latitudes of Eurasia.

We have examined climatological mean and standard deviation of SIC at SO(-1) based on the period from 1979 to 2014 (not shown, please see Figures S2–S3). Large climatological mean SO(-1) SIC is observed in the polar region and off the north coast of Canada and Greenland, and relatively small SIC appears in the marginal seas (Figs. S2a and S3a). In addition, it is interesting to note that large standard deviation (i.e., large interannual variability) of SO(-1) SIC (Figs. S2b and S3b) is observed in regions where significant positive SO(-1) SIC anomalies are detected (Fig. 3a). We have also analyzed the leading EOF modes of interannual variability of SO(-1) Arctic SIC during 1979–2014 (not shown, please see Figures S4–S5). The spatial structure of the first EOF mode of SO(-1) SIC (Figs. S4a and S5a) is highly similar to that in Fig. 3a. These results imply that the Arctic SIC change during preceding early autumn may be indicative of the mid-high latitude Eurasian SAT variations during the following spring.

Based on the distribution of significant negative SIC anomalies in Fig. 3a, we define a SIC index using area-averaged SO(-1) SIC anomalies over the domain of  $71^{\circ}$ – $79^{\circ}$ N and  $105^{\circ}$ E– $120^{\circ}$ W. Figure 4 displays the normalized original SO(-1) SIC index (Fig. 5a) together with its interannual component (Fig. 4b). A significant decreasing trend is observed in the original SO(-1) SIC index, especially after the late-1990s. The normalized original SO(-1) SIC anomalies are above (below) zero during most years before (after) the late-1990s. This is consistent with previous studies (Comiso et al. 2008; Francis et al. 2009; Hopsch et al. 2012; Wu et al. 2012). These previous studies showed that the autumn Arctic sea ice has been declining in the past several decades, and the decline is accelerated after the late 1990s. As shown in Fig. 4b, the interannual variability of SO(-1) SIC seems to have increased since the 1990s. Very similar results are obtained when using SIC data from the NSIDC (Figure S6). The reason for the increased interannual variability in SO(-1) SIC remains to be explored in the future. The present study focuses on analyzing the linkage

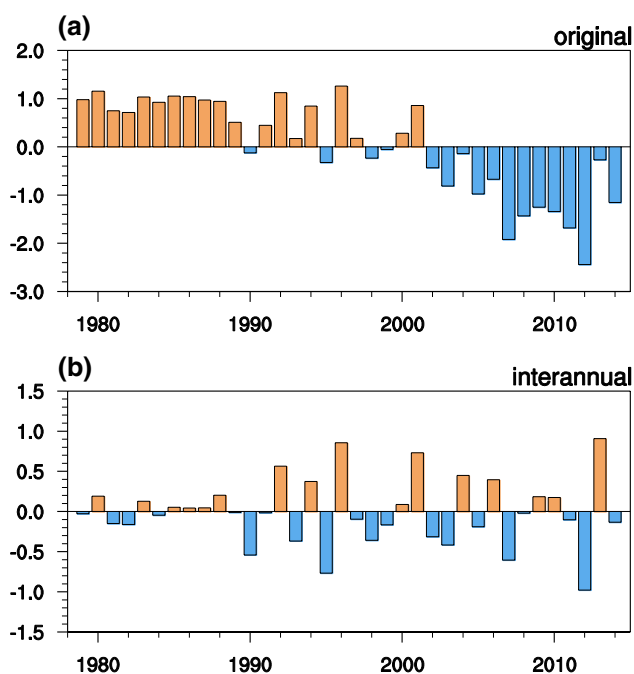


**Fig. 4** **a** The normalized time series of original  $SO(-1)$  SIC index. **b** Interannual component of  $SO(-1)$  SIC index. The SIC index is defined as area-averaged SIC anomalies over the domain of  $71^{\circ}$ – $79^{\circ}$ N and  $105^{\circ}$ E– $120^{\circ}$ W as shown in Fig. 3a. SIC data were derived from the HadISST

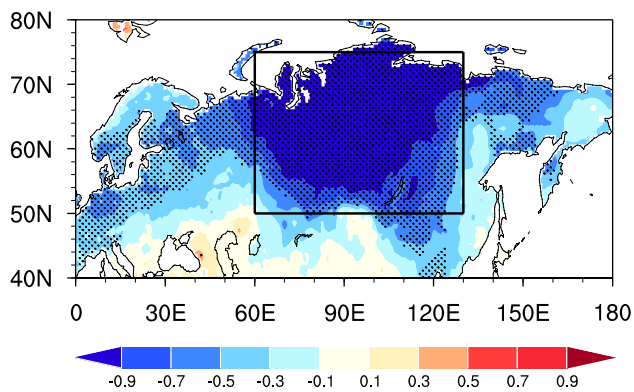


**Fig. 5** Anomalies of surface air temperature (unit:  $^{\circ}$ C) in MA(0) regressed upon the normalized minus one  $SO(-1)$  SIC index. Stippling regions indicate anomalies that significantly different from zero at the 95% confidence level. The black box denotes regions used for constructing spring Eurasian SAT index in Fig. 17

between Arctic SIC and spring Eurasian SAT variations on the interannual timescale.

The connection between preceding early autumn Arctic SIC and subsequent spring Eurasian SAT variations is confirmed by analysis with the  $SO(-1)$  SIC index as reference. Figure 5 displays spring SAT anomalies over the mid-high latitudes of Eurasian continent obtained by regression on the normalized  $SO(-1)$  SIC index. Here and for the remainder

of this study, regression coefficients are multiplied by  $-1$  so that anomalies correspond to low  $SO(-1)$  SIC index year. Pronounced negative spring SAT anomalies are observed over most parts of the Eurasian mid-high latitudes, with largest negative anomalies over central Siberia and north coast of Russia. The distribution is quite similar to that of the leading EOF mode of spring SAT (Fig. 1a).

The distribution of atmospheric circulation anomalies with respect to the low  $SO(-1)$  SIC index is similar to that corresponding to the leading spring SAT mode. Figure 6 displays anomalies of SLP, 850-hPa winds, 500 and 200-hPa geopotential height regressed upon the normalized minus one  $SO(-1)$  SIC index. Corresponding to low  $SO(-1)$  SIC index, there are significant positive SLP and geopotential height anomalies over the high latitudes and significant negative anomalies over east Europe and east Asia (Fig. 6a, c, d). At 850-hPa, two significant anomalous cyclones appear over East Europe and northeast Asia, together with significant anomalous easterly winds over East Europe around  $60^{\circ}$ N and anomalous northeasterly winds over the mid-high latitudes of Eurasian continent (Fig. 6b). The anomalous northeasterly winds bring colder air from the higher latitudes, contributing to the formation of large negative SAT anomalies (Fig. 5). Furthermore, based on Chen et al. (2016a), the anomalous cyclone over northeast Asia may increase cloud cover so that less downward shortwave radiation reaches the surface, contributing partly to negative SAT anomalies there.

#### 4 Possible physical processes linking autumn SIC with spring Eurasian SAT

Previous section indicates a connection between preceding early autumn Arctic SIC and spring Eurasian SAT variations. In this section, we investigate the plausible physical processes connecting the  $SO(-1)$  SIC to the following spring Eurasian SAT variations. Previous study has demonstrated that spring AO plays a dominant role in the variation of the spring SAT over the mid-high latitudes of Eurasia primarily via wind-induced temperature advection (Chen et al. 2016a). Hence, it is reasonable to infer that the impact of  $SO(-1)$  SIC on the following spring Eurasian SAT may be through modulating the spring AO.

Here, we examine and compare atmospheric anomalies in association with  $SO(-1)$  SIC and spring AO index. Figure 7 displays anomalies of SLP, 850-hPa winds, 500 and 200-hPa geopotential height regressed upon the normalized minus one spring AO index. Apparently, atmospheric circulation anomalies related to negative phase of spring AO bear a close resemblance to those related to low  $SO(-1)$  SIC index year (Figs. 6, 7). The correlation coefficient between  $SO(-1)$  SIC index and spring AO index reaches 0.5 during 1979–2014, significant at the 99% confidence

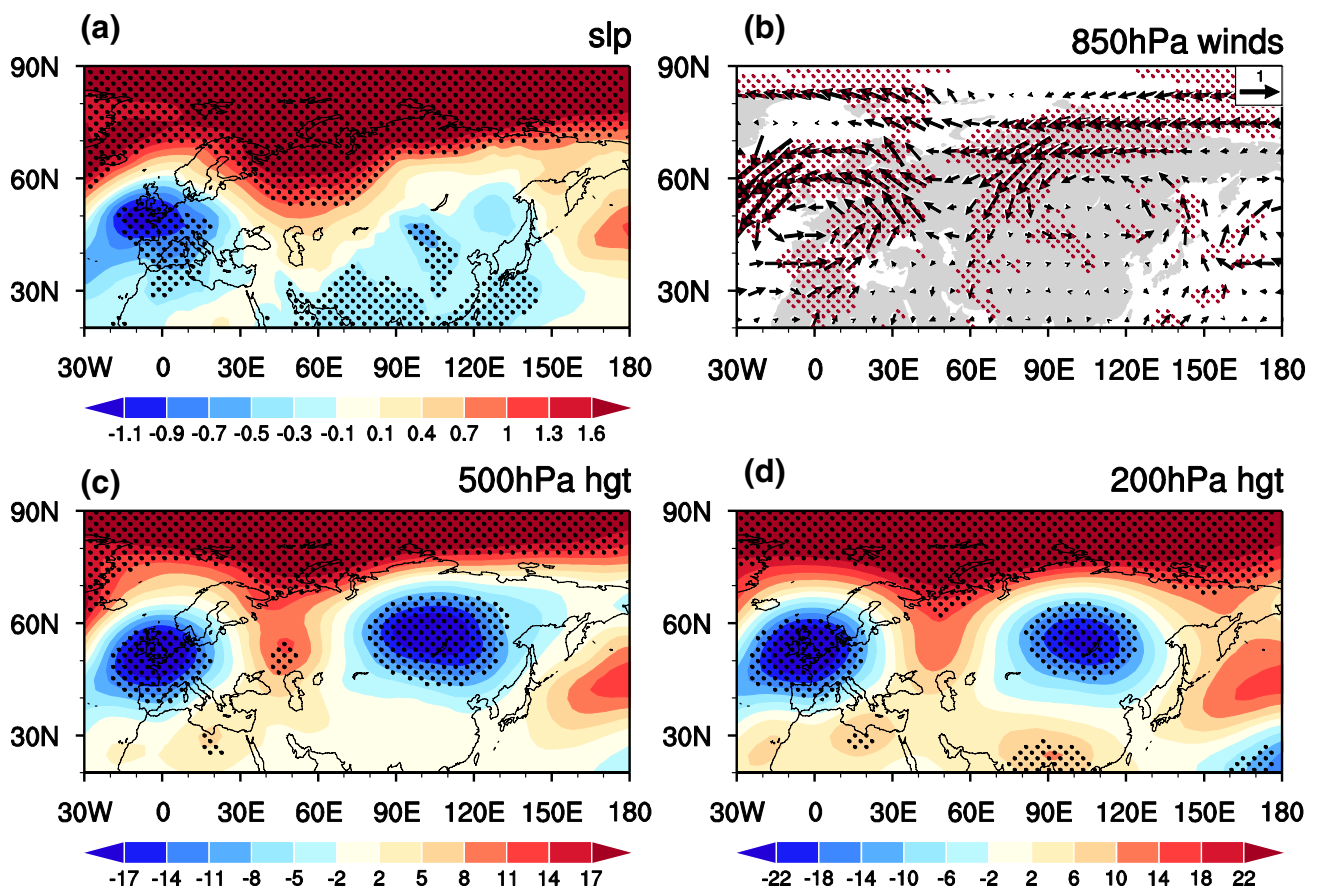


**Fig. 6** As in Fig. 2, but for anomalies at spring regressed upon the normalized minus one  $SO(-1)$  SIC index

level according to the Student's  $t$  test. In the negative phase of spring AO, significant positive SLP and geopotential height anomalies are observed over the high latitudes and significant negative anomalies are present over east Europe and East Asia (Fig. 7a, c, d). Note that the center of negative geopotential height anomalies over East Asia is located more northward compared to the center of negative SLP anomalies (Fig. 7a, c, d). These are consistent with results presented in Fig. 6. At 850-hPa, two significant anomalous cyclones are present over East Europe and northeast Asia with significant anomalous easterly winds over East Europe around  $60^{\circ}N$  and anomalous northeasterly winds over the mid-high latitudes of Eurasian continent (Fig. 7b).

Figure 8a, b display the vertical structures of spring zonal wind anomalies averaged over the Eurasian sector in association with the low  $SO(-1)$  SIC and negative phase of spring AO index, respectively. It is obvious that zonal wind anomalies related to both  $SO(-1)$  SIC index and spring AO index display an equivalent barotropic dipole structure, with enhanced westerlies around  $40^{\circ}N$  and reduced westerlies around  $70^{\circ}N$ . The wind anomalies extend from the surface to the lower stratosphere with the magnitude increasing with the altitude (Fig. 8).

Above results suggest that spring AO may play an important role in relaying the influence of  $SO(-1)$  SIC on the subsequent spring Eurasian SAT. To further confirm the role of spring AO, we first remove the spring AO index from the  $SO(-1)$  SIC index by a linear regression and then regress the spring SAT and SLP anomalies into the normalized  $SO(-1)$  SIC index. The obtained anomalies are presented in Fig. 9. Apparently, spring SAT and SLP anomalies over Eurasia become insignificant and extremely weak after removing the signal of spring AO. This verifies the speculation that the change in  $SO(-1)$  SIC influences spring AO and the atmospheric circulation anomalies related to spring AO further affect spring SAT anomalies over the mid-high latitudes of Eurasian continent.

A question that needs to be addressed is: What are the physical processes for the influence of  $SO(-1)$  SIC on subsequent spring AO? Several previous studies have demonstrated that the stratospheric process plays a crucial role in the impacts of the Arctic sea ice on the AO-like atmospheric circulation changes (e.g., Jaiser et al. 2012; Kim et al. 2014; Nakamura et al. 2015; King et al. 2016; Yang et al. 2016). According to these studies, upward propagation of stationary planetary waves into the stratosphere is enhanced (reduced)

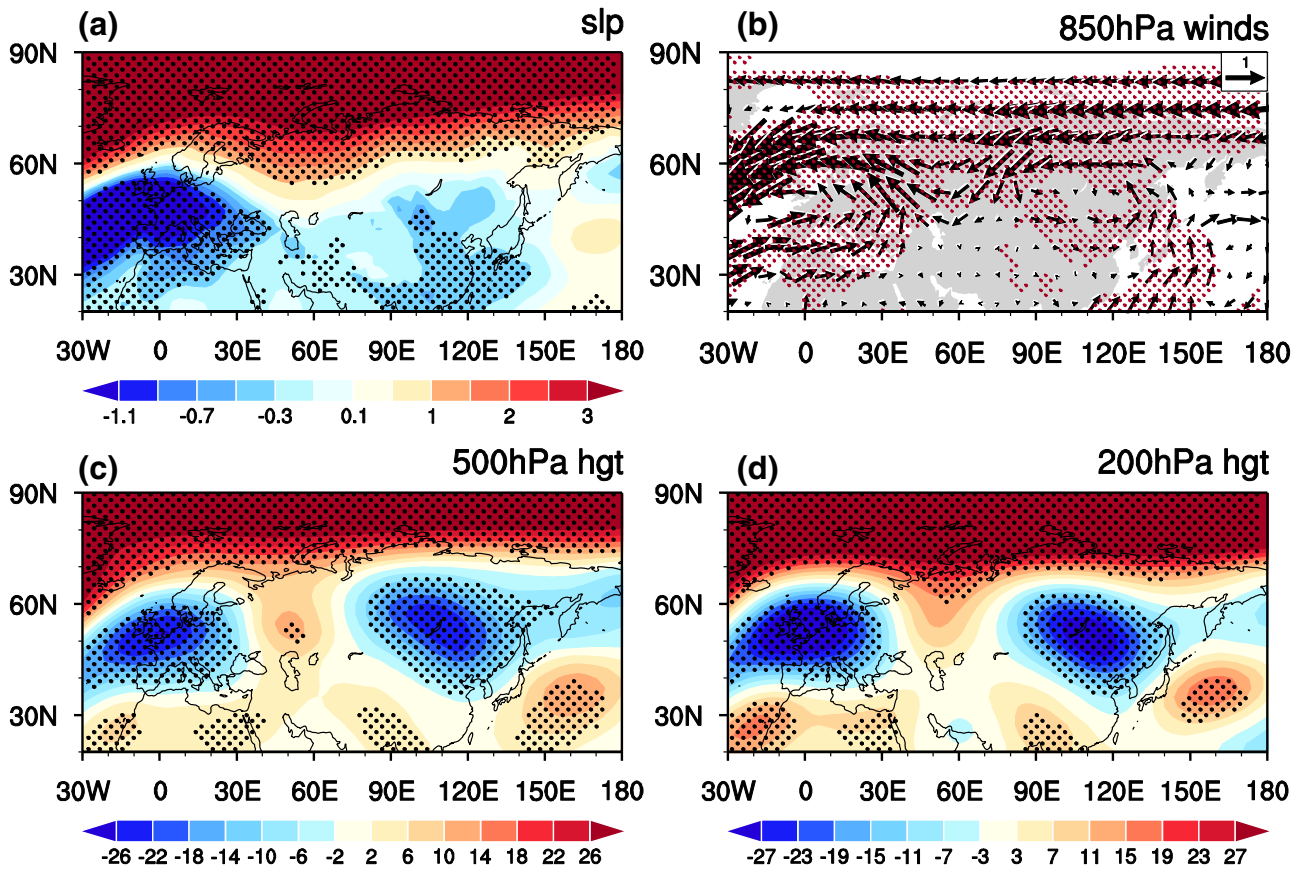
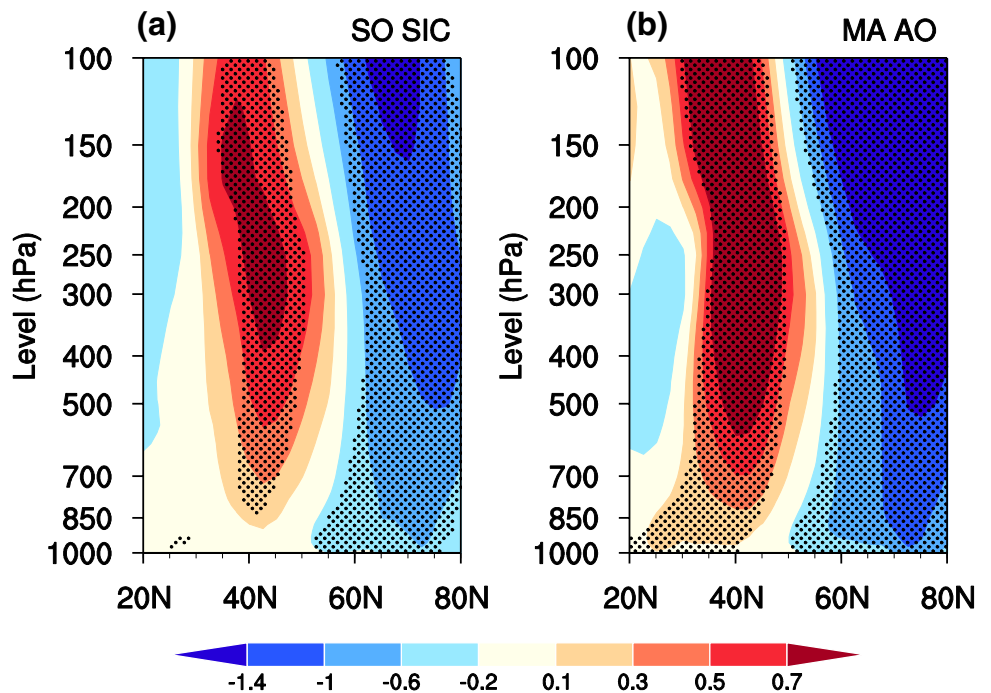
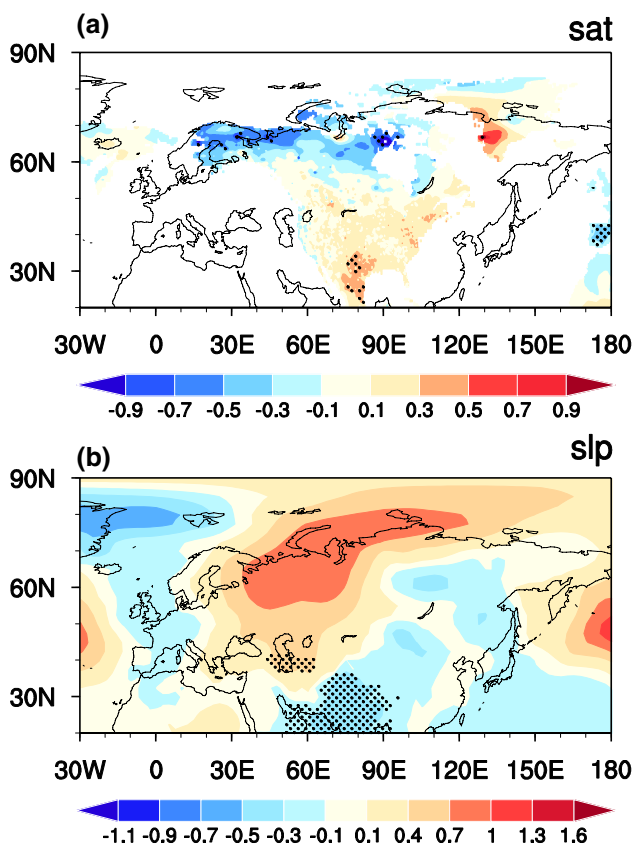


Fig. 7 As in Fig. 2, but for anomalies at spring regressed upon the normalized minus one spring AO index (i.e., negative phase of spring AO)

Fig. 8 Height-latitude cross sections of spring zonal wind (unit:  $m s^{-1}$ ) anomalies over Eurasia ( $0-140^{\circ}E$ -averaged) regressed upon the normalized minus one **a** SO(-1) SIC index and **b** spring AO index. Stippling regions indicate anomalies that significantly different from zero at the 95% confidence level







**Fig. 9** Anomalies of spring **a** SAT (unit: °C) and **b** SLP (unit: hPa) regressed upon the normalized minus one SO(-1) SIC index. Note that the normalized spring AO index has been subtracted from the normalized SO(-1) SIC index by linear regression before constructing this figure. Stippling regions indicate anomalies that significantly different from zero at the 95% confidence level

when the Arctic sea ice is below (above) normal. The EP flux convergence (divergence) associated with the increase (decrease) in upward propagating planetary waves leads to deceleration (acceleration) of the stratospheric zonal winds over the mid-high latitudes of the NH, indicating a weakening (strengthening) of the stratospheric polar vortex. Then, through the coupling between stratosphere and troposphere and downward propagation of zonal wind anomalies, a negative (positive) AO pattern is formed in the troposphere. In addition, previous studies have revealed that AO in the troposphere is closely related to the change in the polar vortex in the stratosphere (Baldwin and Dunkerton 1999, 2001; Ambaum and Hoskins 2002; Polvani and Waugh 2004).

Obvious signals are detected in the stratosphere in association with autumn Arctic sea ice changes. Figure 10 displays evolution of zonal mean zonal wind anomalies (averaged over 60°–80°N) and geopotential height anomalies (averaged over 70°–90°N) obtained by regression upon the normalized minus one SO(-1) SIC index. At ON(-1) and ND(-1), significant anomalous easterly winds are observed over the

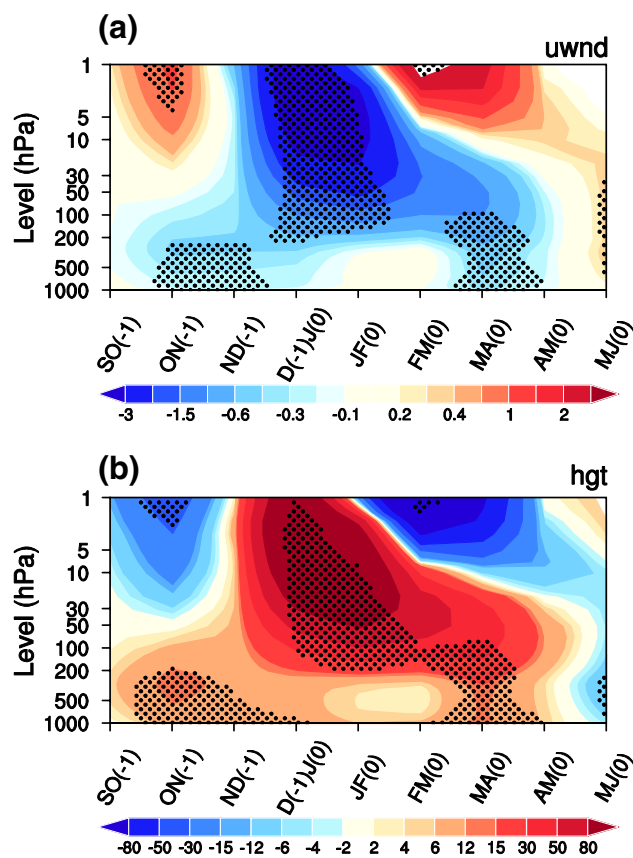


**Fig. 10** Evolution of **a** zonal mean zonal wind anomalies (averaged over 60°–80°N) and **b** zonal mean geopotential height anomalies (averaged over 70°–90°N) obtained by regression upon on the normalized minus one SO(-1) SIC index. Stippling regions indicate anomalies that significantly different from zero at the 95% confidence level

mid-high latitudes extending from 1000-hPa to around 200-hPa (Fig. 10a). Formation of these easterly wind anomalies will be discussed later. Correspondingly, there are pronounced positive geopotential height anomalies over the mid-high latitudes of the NH (Fig. 10b). Deceleration of zonal mean zonal winds and development of positive geopotential height anomalies are detected in the stratosphere at ND(-1), indicating a weakening of the polar vortex. These anomalous easterly winds and associated positive geopotential height anomalies in the stratosphere propagate downward and reach the lower troposphere at MA(0). Hence, a negative AO pattern is formed in the troposphere at MA(0). Above results demonstrated that the impact of SO(-1) Arctic sea ice on the subsequent spring AO variability may be partly through the stratospheric pathway.

Formation of the easterly wind anomalies at ND(-1) in the stratosphere may be attributed to the anomalous upward propagation of planetary waves excited by SIC loss, as described below. Before investigating the stationary planetary wave activity related to the SO(-1) SIC, we first show

climatological distributions of the stationary planetary wave as a background for the later analysis. Figure 11 displays climatological distribution of the EP flux and its divergence for the sum of zonal wave numbers 1–3 from SO(–1) to MA(0) for period 1979–2014. It shows that stationary planetary waves propagate vertically from lower troposphere at mid-latitudes, then separate into two branches around the upper troposphere, with one going upward into the stratosphere and the other propagating equatorward in the troposphere (Fig. 11). Upward propagations of stationary planetary waves are much weaker at SO(–1) and MA(0) (Fig. 11a g)

compared to those at ON(–1), ND(–1), JF(0), FM(0) (Fig. 11b–f). In addition, most regions of the mid-high latitudes of troposphere and stratosphere are dominated by EP flux convergence (Fig. 11). Correspondingly, amplitudes of the EP flux convergence are also much weaker at SO(–1) and MA(0) (Fig. 11a g). The above results are generally consistent with previous studies (Huang and Gambo 1983; Chen et al. 2003).

Figure 12 displays anomalies of EP flux and EP flux divergence from SO(–1) to MA(0) (sum of wavenumbers 1–3) obtained by regression upon the normalized SO(–1)

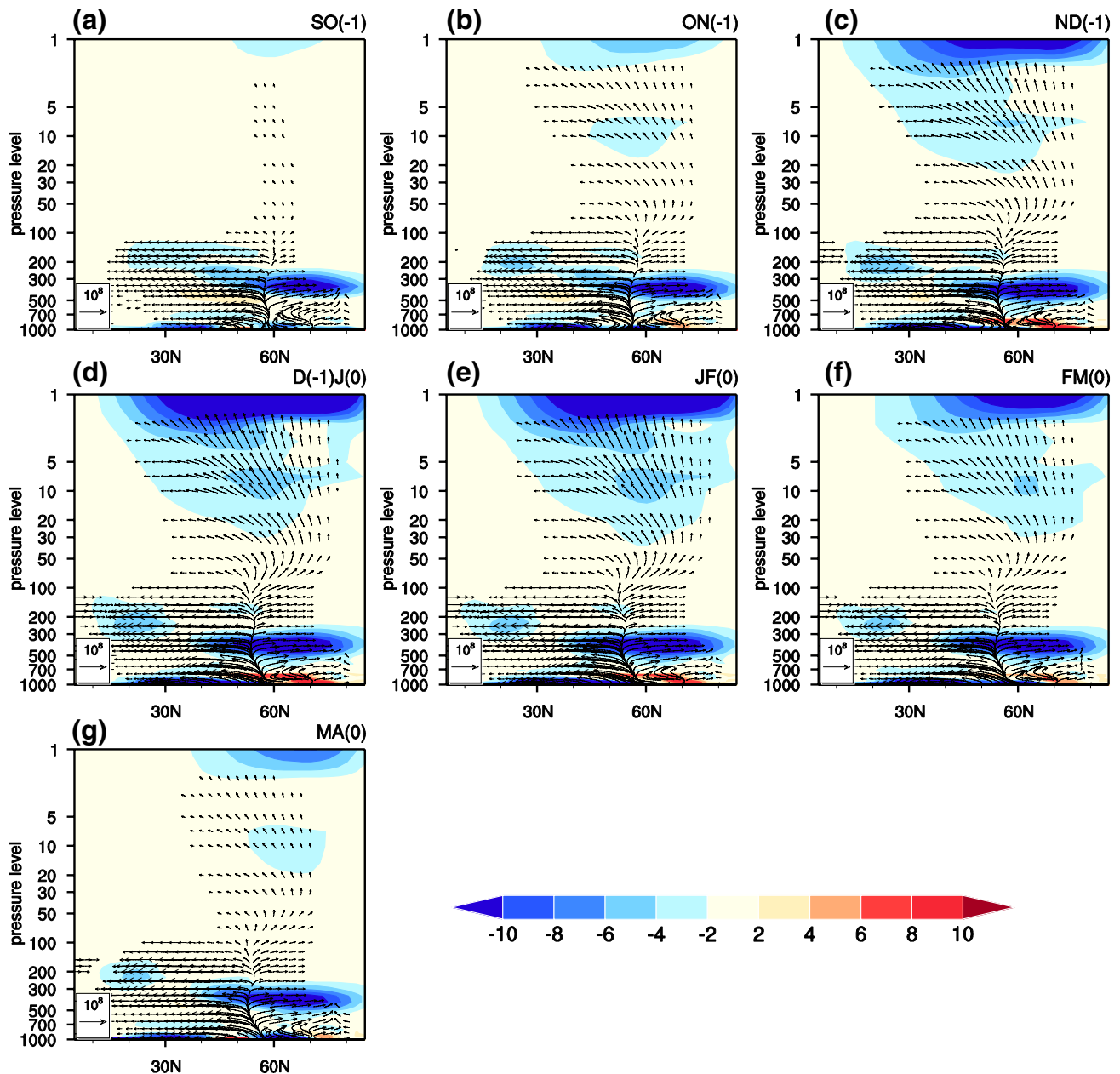


**Fig. 11** Climatology of the EP flux (vector; unit:  $\text{m}^2 \text{s}^{-2}$ ) and its divergence (shading; unit:  $\text{m s}^{-2}$ ) at **a** SO(–1), **b** ON(–1), **c** ND(–1), **d** D(–1)J(0), **e** JF(0), **f** FM(0), and **g** MA(0), respectively, based on the period from 1979 to 2014

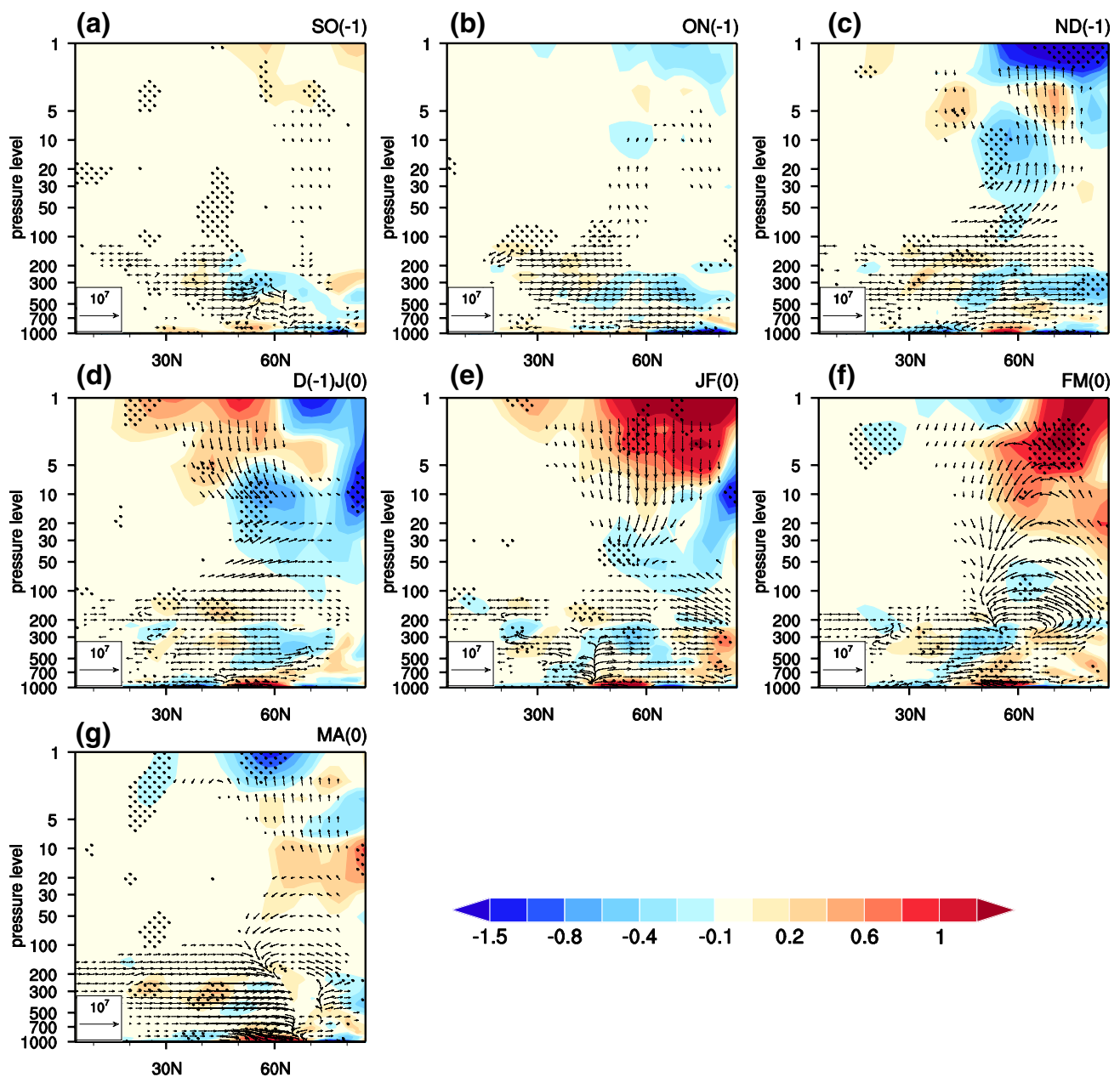


**Fig. 12** Anomalies of EP flux (vector; unit:  $\text{m}^2 \text{s}^{-2}$ ) and its divergence (shading; unit:  $\text{m s}^{-2}$ ) at **a** SO(-1), **b** ON(-1), **c** ND(-1), **d** D(-1) J(0), **e** JF(0), **f** FM(0), and **g** MA(0), respectively, obtained by regres-

sion upon the normalized minus one SO(-1) SIC index. Stippling regions indicate EP flux divergence anomalies that significantly differ from zero at the 95% confidence level

SIC index. EP flux anomalies are generally weak over mid-high latitudes of the stratosphere at SO(-1) and ON(-1) (Fig. 12a, b). At ND(-1), strong anomalous upward propagation of stationary planetary waves are observed over mid-high latitudes from the upper troposphere to the stratosphere (Fig. 12c). This is accompanied by pronounced EP flux convergence anomalies around  $60^{\circ}$ – $80^{\circ}$ N over large parts of the stratosphere. Thereby, easterly wind anomalies are induced in the stratosphere over the mid-high latitudes of the NH (Fig. 10a) as convergence of EP flux results in the

deceleration of zonal winds according to the wave-mean flow interaction theory (e.g., Andrews et al. 1987; Holton 2004; Vallis 2006). Correspondingly, the polar vortex weakened at ND(-1) (Fig. 10). There exists downward EP flux anomalies and associated EP flux divergence anomalies from D(-1) J(0) to FM(0) over the mid-high latitudes (Fig. 12d–f). These correspond well to the downward propagation of the zonal mean zonal wind and geopotential height anomalies from the stratosphere (Fig. 10), generally consistent with previous findings (Christiansen 2001; Wang and Chen 2010; Yang

et al. 2016). Previous studies have reported that downward propagations of AO signal from the stratosphere are generally associated with preceding anomalous upward EP flux propagation (Christiansen 2001; Wang and Chen 2010; Yang et al. 2016). Baldwin and Dunkerton (2001) showed that it may take more than two months for the atmospheric circulation anomalies to propagate from 10 hPa to the lower stratosphere. In addition, the stratospheric response may persist for several months, accompanied by downward migration to the troposphere. Note that the mechanism of downward migration from the stratosphere to the troposphere has been discussed in previous studies (e.g., Baldwin and Dunkerton 2001; Perlwitz and Harnik 2003; Song and Robinson 2004; Simpson et al. 2009), but was still unclear and remained to be explored.

The increase in the upward propagation of planetary waves into the stratosphere at ND(-1) (Fig. 12) may be related to the deceleration of westerly winds in the troposphere extending from 1000 to 200-hPa at ON(-1) (Fig. 10a). Based on the *Charney-Drazin* criterion for Rossby waves to propagate vertically (e.g., Charney and Drazin 1961; Mohanakumar 2008), and the findings of previous studies (e.g., Chen et al. 2002, 2003), decrease in the prevailing westerly winds in the mid-high latitudes of troposphere is more favorable for the upward propagation of planetary waves into the stratosphere. We define a zonal mean zonal wind index to further confirm role of the prevailing westerly wind change over the mid-high latitudes of troposphere in influencing the upward propagation of the stationary wave. According to the pattern shown in Fig. 10a, the zonal wind index (ZWI) is defined as zonal mean zonal wind anomalies at ON(-1) averaged over the domain of 60°–80°N and 850–200 hPa. Figure 13 displays anomalies of ND(-1) EP flux and its divergence obtained by regression on the normalized ON(-1) ZMI. Regression coefficients in Fig. 13 are multiplied by -1 so that anomalies correspond to easterly wind anomalies (i.e., deceleration of prevailing westerly winds). It is clear that anomalous upward propagation of stationary wave and associated EP flux convergence anomalies appear in the stratosphere at the mid-high latitudes corresponding to weakened prevailing westerly winds at the mid-high latitudes of the troposphere. This is in agreement with previous studies (Charney and Drazin 1961; Chen et al. 2003; Mohanakumar 2008).

Here, another question that needs to be addressed is: How are anomalous easterly wind anomalies formed around 60°–80°N in the mid-high latitudes of the troposphere? The formation of anomalous easterly winds may be related to the decrease in the meridional temperature gradient and atmospheric thickness in response to the decrease in the Arctic SIC, as has been discussed by previous studies (e.g., Liu et al. 2012a, b; Francis and Vavrus 2012; Sun et al. 2016b).

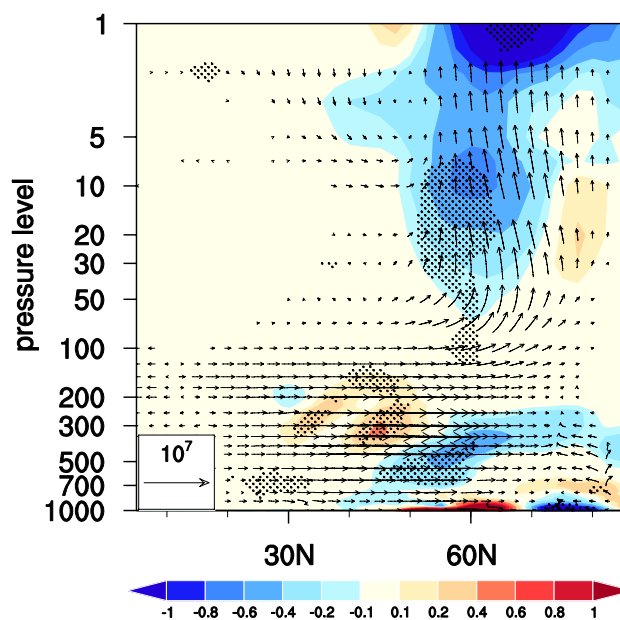


**Fig. 13** Anomalies of ND(-1) EP flux (vector, unit:  $\text{m}^2 \text{s}^{-2}$ ) and its divergence (shading, unit:  $\text{m s}^{-2}$ ) regressed upon the normalized ON(-1) ZMI. Definition of ZMI are provided in the text. Regression coefficients are multiplied by -1 so that anomalies correspond to minus one standard deviation of ON(-1) ZWI (i.e., easterly wind anomalies). Stippling regions indicate EP flux divergence anomalies that significantly different from zero at the 95% confidence level

Figure 14a displays height-latitude cross sections of zonal mean temperature anomalies at SO(-1) and zonal wind anomalies at ON(-1) regressed upon the normalized minus one SO(-1) SIC index. Significant positive temperature anomalies are observed around 70°–90°N extending from 1000 to around 400-hPa in response to less SO(-1) SIC. Hence, easterly wind anomalies are induced over the mid-high latitudes due to the decrease of the meridional temperature gradient based on the thermal-wind balance relation. The positive temperature anomalies over the high latitudes may be attributed to the sea ice-albedo effect. Less sea ice reflects less downward shortwave radiation (not shown). This results in an increase in shortwave radiation reaching the surface and favors positive temperature anomalies. We have also examined atmospheric thickness changes in association with SO(-1) SIC index. Figure 14a displays zonal mean 1000–200 hPa atmospheric thickness anomalies at SO(-1) regressed upon the normalized SO(-1) SIC index. For comparison, climatological distribution of the 1000–200 hPa atmospheric thickness is also provided in Fig. 14b. The mean 1000–200 hPa atmospheric thickness decreases toward the North pole, consistent with the distribution of climatological air temperature (not shown). Large increase in 1000–200 hPa atmospheric thickness appears over the mid-high latitudes corresponding to less SIC. Hence, the meridional thickness gradient over Eurasia

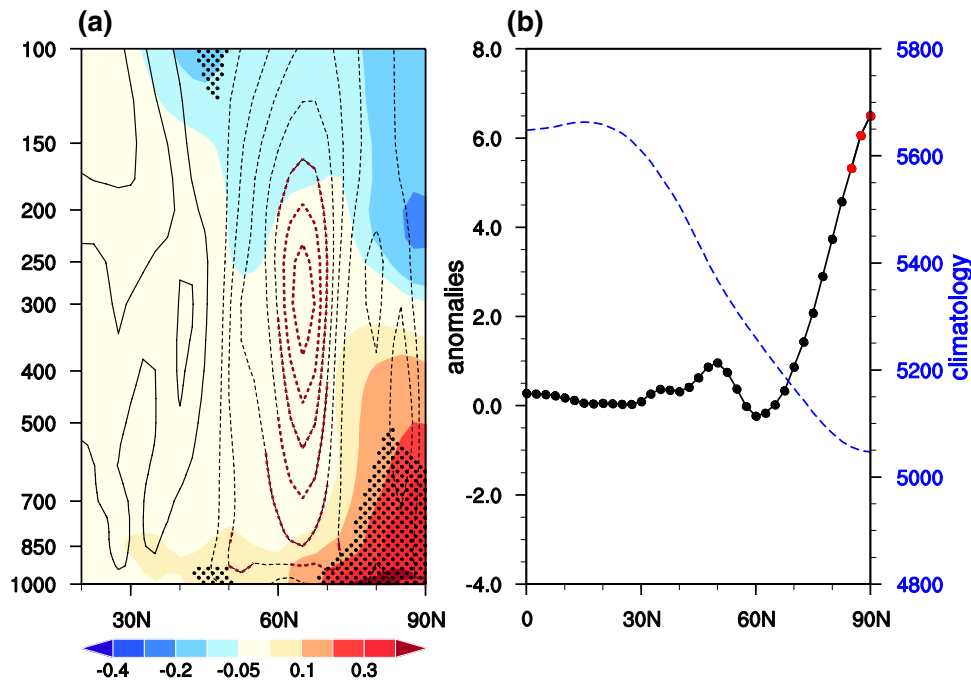


**Fig. 14** **a** Height-latitude cross sections of zonal mean air temperature ( $^{\circ}\text{C}$ ) at  $\text{SO}(-1)$  and zonal mean zonal wind anomalies ( $\text{m s}^{-1}$ ) at  $\text{ON}(-1)$  regressed upon the normalized minus  $\text{SO}(-1)$  SIC index. Stippling (red contour) in **a** indicates air temperature (zonal wind) anomalies significant at the 95% confidence level. Contour interval for zonal wind is  $0.1 \text{ m s}^{-1}$ , and zero line is omitted. Solid (dashed) lines indicate westerly (easterly) wind anomalies. **b** Climatologi-

cal distribution of zonal mean 1000–200 hPa atmospheric thickness (m) at  $\text{SO}(-1)$  (blue dashed line). Anomalies of zonal mean 1000–200 hPa atmospheric thickness (m) at  $\text{SO}(-1)$  regressed upon the normalized minus one  $\text{SO}(-1)$  SIC index (black dotted line). Red dot in **b** indicates anomalies significantly different from zero at the 95% confidence level

decreases. As indicated by previous studies (e.g., Francis and Vavrus 2012; Sun et al. 2016b), decrease in the meridional gradient of the thickness over the mid-high latitudes may lead to a decrease in prevailing westerly winds. Therefore, the formation of  $\text{ON}(-1)$  easterly wind anomalies in the troposphere around  $60^{\circ}$ – $80^{\circ}\text{N}$  may be related to the decrease in the meridional temperature and thickness gradient.

## 5 Autumn Arctic SIC-spring SAT connection in a coupled model historical simulation

In this section, we examined the reproducibility of the observed connection in a historical simulation of the flexible global ocean-atmosphere-land system model, spectral version 2 (FGOALS-s2) (Bao et al. 2013). FGOALS-s2 is a state-of-the-art fully coupled global climate model developed by the State Key Laboratory of Numerical Modeling for Atmospheric Sciences and Geophysical Fluid Dynamics (LASG) at the Institute of Atmospheric Physics (IAP), Chinese Academy of Sciences (CAS). FGOALS-s2 has four components, atmosphere, ocean, sea ice, and land. Its atmospheric component is a Spectral Atmospheric Model in IAP LASG version 2 (SAMIL2), which has a horizontal

resolution of approximately  $2.81^{\circ} \times 1.66^{\circ}$  (longitude  $\times$  latitude) and 26 levels in the vertical direction (Bao et al. 2013). Its ocean component is Climate System Ocean Model version 2 (LICOM2) in LASG IAP, which has a horizontal resolution of approximately  $0.5^{\circ} \times 0.5^{\circ}$  over the tropical region and about  $1^{\circ} \times 1^{\circ}$  over the extratropics (Liu et al. 2012a, b; Lin et al. 2013). The sea ice and land components are Community Sea Ice Model version 5 (Collins et al. 2006) and Community Land Model version 3 (Oleson et al. 2004), respectively. More detailed information of the FGOALS-s2 is referred to Bao et al. (2013).

The FGOALS-s2 simulation examined here is the historical experiments integrated from 1850 to 2005 under historical forcing, including greenhouse gases, solar radiation cycle, sulfate aerosols, etc. Definitions of the  $\text{SO}(-1)$  Arctic SIC index and spring AO index in the FGOALS-s2 are the same as those in the observations. In addition, all the analyzed variables are subjected to a 7 year high pass Lanczos filter, too. The simulated relation between autumn Arctic SIC and following spring Eurasian SAT was firstly examined. Figure 15a, b display anomalies of  $\text{SO}(-1)$  Arctic SIC and subsequent spring surface temperature over Eurasian, respectively, obtained by regression upon the minus one  $\text{SO}(-1)$  SIC index in the historical simulations

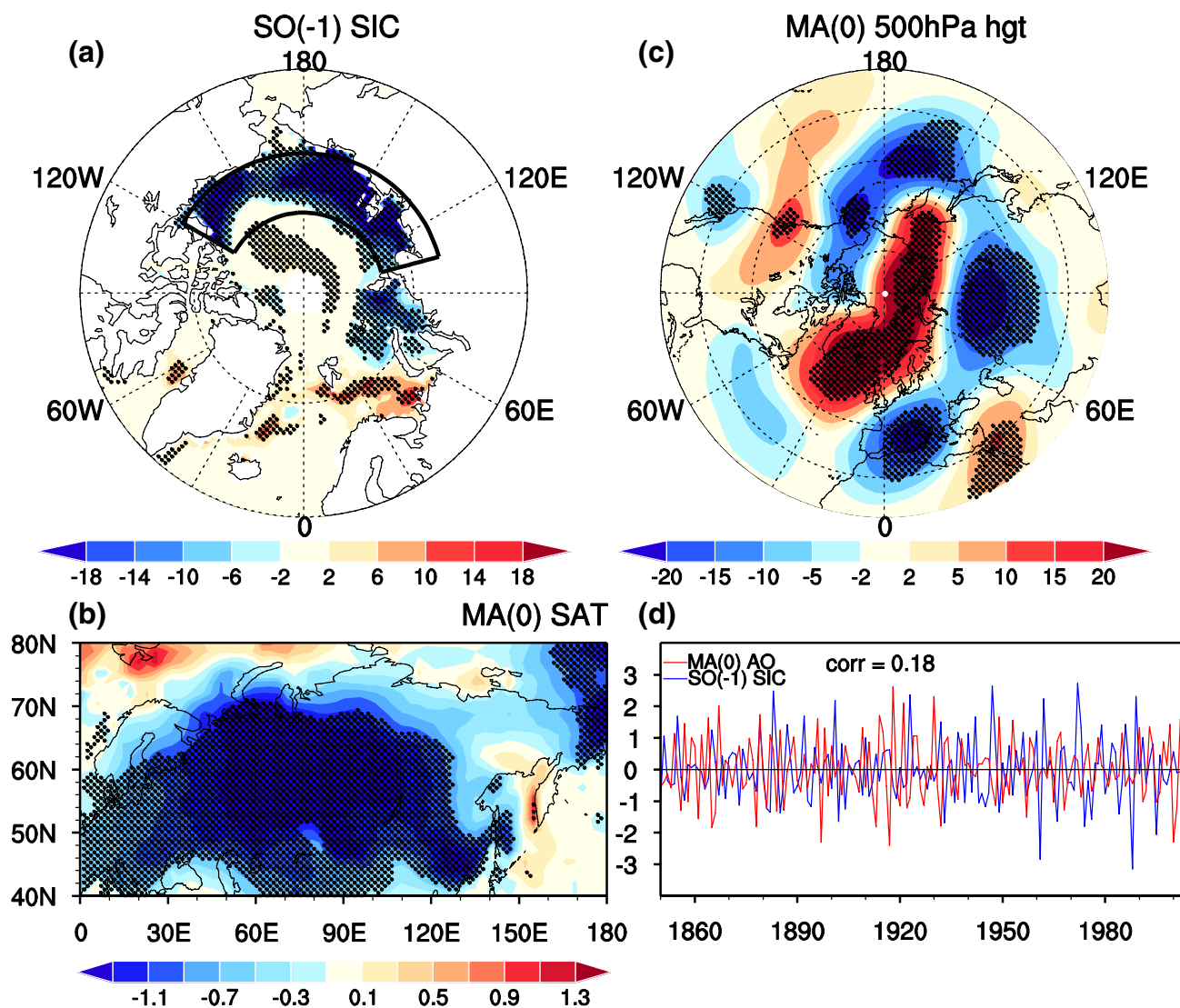


**Fig. 15** Anomalies of **a** SO(-1) SIC, **b** MA(0) surface temperature, **c** 500 hPa geopotential height obtained by regression upon the minus one SO(-1) SIC index in the historical simulations of FGOALS-s2 for period 1850–2004. **d** Normalized time series of SO(-1) SIC index and subsequent spring AO index in the historical climate sim-

ulations of FGOALS-s2 for period 1850–2004. Stippling regions in **a–c** indicate anomalies significantly different from zero at the 95% confidence level. Definitions of the SO(-1) SIC index (averaged over the black box region in **a**) and spring AO index in FGOALS-s2 are to the same as those defined in the observation

of FGOALS-s2 for period 1850–2004. Notable negative surface temperature anomalies appear over most parts of the Eurasian continent (Fig. 15b) when there is less SIC in the Laptev Sea-eastern Siberian Sea-Beaufort Sea (Fig. 15a). This indicates that the FGOALS2-s2 well reproduces the observed autumn Arctic SIC-spring Eurasian SAT connection (Figs. 5, 15a, b). As we have indicated in the observation that influence of the autumn SIC on the subsequent spring Eurasian SAT is via inducing a spring AO-like atmospheric circulation anomalies, the atmospheric circulation anomalies in spring related to preceding autumn Arctic SIC index were further examined. Figure 18c displays spring 500 hPa geopotential height anomalies regressed upon the

preceding Autumn SIC index simulated by the FGOALS-s2 for period 1850–2004. 500 hPa geopotential height anomalies show a marked meridional seesaw pattern, which bears a resemblance to that related to the negative phase of the AO (Thompson and Wallace 1998; Chen et al. 2014a), with significant negative anomalies over mid-latitudes and positive anomalies over Arctic (Fig. 15c). In particular, correlation coefficient between the autumn Arctic SIC index and spring AO index is 0.18 during 1850–2004 (Fig. 15d), significant at the 95% confidence level according to the two-tailed Student's *t* test. Above analyses indicate that the FGOALS-s2 can generally simulate the observed connection between preceding autumn Arctic SIC anomalies in the

Laptev Sea-eastern Siberian Sea-Beaufort Sea and following spring Eurasian surface temperature change via modulating the spring AO.

Then, we examined temporal evolutions of the zonal mean zonal wind and geopotential height anomalies from autumn to subsequent spring, which are presented in Fig. 16. Similar to observation (Fig. 10), it seems that the formation of the atmospheric anomalies signals in the lower troposphere is related to the downward propagating anomalies from the stratosphere (Fig. 16), though the FGOALS-s2 has a lower pressure top (10 hPa) than that in the observations (1 hPa). In addition, it seems that the formation of the easterly wind anomalies over mid-latitudes of NH as a response to the SIC loss is faster in the FGOALS-s2 simulation [SO(- 1)] that that in the observations [ON(- 1)]. Generally, above evidences indicate that the stratospheric process may also play an important role in relaying the influence of the preceding autumn Arctic SIC on the following spring AO in the FGOALS-s2 simulation, which further leads to change in the surface temperature anomalies over the Eurasian continent (Chen et al. 2016a). The similarity between the FGOALS-s2 simulation and observation confirm the linkage between autumn Arctic SIC change in the Laptev

Sea-eastern Siberian Sea-Beaufort Sea and the subsequent spring Eurasian SAT variation.

### 6 Empirical model of spring Eurasian SAT

Previous sections have identified a significant impact of preceding autumn SIC in the Laptev Sea-eastern Siberian Sea-Beaufort Sea on the spring SAT variation over mid-high latitudes of Eurasia via modulating the spring AO-like atmospheric circulation anomalies. In the following, a statistical prediction model is constructed to predict the spring Eurasian SAT index based on the preceding SO(- 1) Arctic SIC index and spring AO index. According to the result in Fig. 5, spring Eurasian SAT index is defined as area-averaged SAT anomalies over the region of 50°-75°N and 60°-130°E. The empirical model is shown as follows:

$$SAT(t) = a \times SIC(t) + b \times AO\_res(t).$$

Where *t* denotes time in years. SAT(*t*) is spring Eurasian SAT index, SIC(*t*) is SO(- 1) Arctic SIC index. Because spring AO index has a close relationship with preceding SO(- 1) Arctic SIC index, we subtract the SO(- 1) Arctic SIC signal from spring AO index by mean of linear regression. Hence, AO\_res(*t*) in the above empirical model represents the part of spring AO index that is linearly unrelated to the preceding SO(- 1) Arctic SIC index. The ability of the empirical model is cross validated via a leave-one-out scheme (i.e., excluding one year from the period 1979-2014, determining the regression coefficient via remaining indices and then hindcasting the value for the excluded year) (Ham et al. 2013; Zuo et al. 2016).

The cross validated correlation is 0.58 (0.53) when the SO(- 1) Arctic SIC index (spring AO index) is used to hindcast the Eurasian spring SAT index (Fig. 17). By contrast, if both the SO(- 1) Arctic SIC and spring AO indices are used to hindcast the Eurasian spring SAT index, the cross validated correlation is 0.83, which is higher than that only using SO(- 1) Arctic SIC index or spring AO index to predict the Eurasian spring SAT index (Fig. 17). This implies that the SO(- 1) Arctic SIC index indeed provides additional sources for the prediction of Eurasian spring SAT. This confirms that preceding autumn Arctic SIC in the Laptev Sea-eastern Siberian Sea-Beaufort Sea is a notable factor for the subsequent spring Eurasian SAT variations.

### 7 Summary and discussion

Using atmospheric variables from the ERA-Interim reanalysis, SAT from the University of Delaware, and SIC data from the HadISST and NSIDC for the period 1979-2014, the present study revealed a close connection between

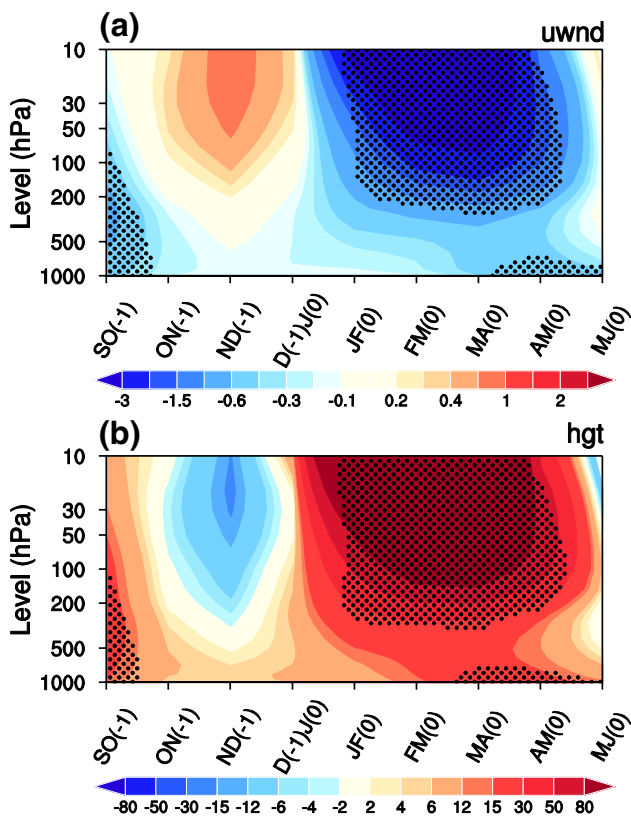
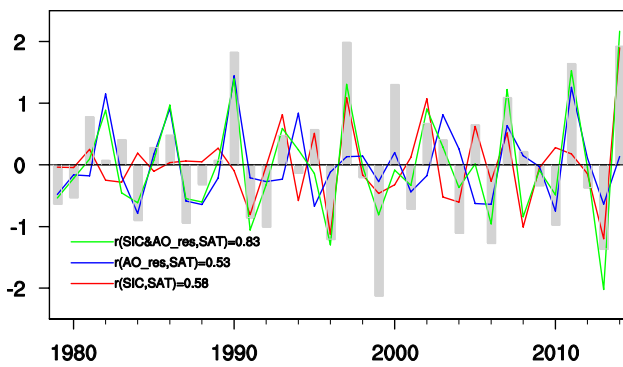


Fig. 16 As in Fig. 10, but for the zonal wind and geopotential height data that are derived from the historical simulations of FGOALS-s2 for period 1850-2004



**Fig. 17** Time series of the spring Eurasian SAT index during 1979–2014 (black bars), and the cross-validated hindcasts of the spring Eurasian SAT index calculated by empirical model using the SO(− 1) Arctic SIC index alone (red line), using the spring AO<sub>res</sub> index alone (blue line), and using both the combined SO(− 1) Arctic SIC index and spring AO<sub>res</sub> index (green line). The correlations between various time series are also provided in the figure. Definitions of the spring Eurasian SAT index, SO(− 1) Arctic SIC index and spring AO<sub>res</sub> index are provided in the text

preceding early autumn (September–October) Arctic SIC and subsequent spring SAT over the mid-high latitudes of Eurasia on the interannual timescale. When the early autumn SIC anomalies are positive (negative) in the regions extending from the Laptev Sea and eastern Siberian Sea eastward to the Beaufort sea, a continental-scale warming (cooling) is observed in the following spring over most parts of the mid-high latitude Eurasia. This indicates that preceding early autumn SIC is a potential predictor for the subsequent

spring SAT variation over the mid-high latitudes of the Eurasian continent.

We further investigated the plausible physical processes for the influence of early autumn Arctic SIC on the following spring Eurasian SAT. Our results indicate that spring AO plays an important role in relaying the impact of early autumn SIC on the subsequent spring Eurasian SAT variation. Furthermore, early autumn Arctic SIC anomalies influence the following spring tropospheric AO variability through the stratospheric pathway. The detailed physical processes connecting early autumn Arctic SIC to subsequent spring SAT over the mid-high latitudes of the Eurasian continent are summarized in Fig. 18 and described below.

When there is less Arctic SIC in the above mentioned Arctic regions in early autumn, significant warming occurs over the high latitudes of the Northern Hemisphere extending from lower to middle troposphere. The warming in the troposphere and the associated increase in air temperature and atmospheric thickness in the high latitudes result in a decrease in the meridional temperature and thickness gradient over the mid-high latitudes, which contributes to the deceleration of circumpolar prevailing westerlies in the troposphere. Anomalous upward propagation of planetary waves into the stratosphere over the high latitudes is induced due to the deceleration of tropospheric prevailing westerly winds. The associated EP flux convergence leads to the deceleration of westerly winds in the stratosphere and the weakening of the polar vortex. Through the coupling between stratosphere and troposphere and downward propagation of anomalous zonal winds, a negative spring AO pattern is formed in the

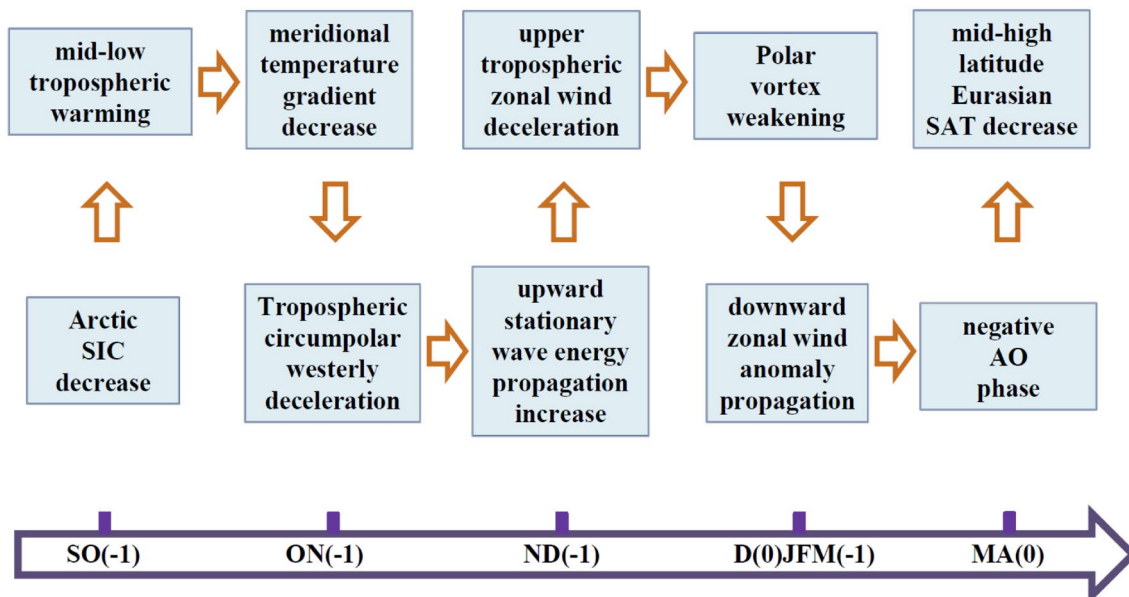


**Fig. 18** Schematic diagram depicting the physical processes responsible for the influence of SO(− 1) SIC on the subsequent spring Eurasian SAT. The time sequence from preceding autumn to following spring is indicated at the bottom



troposphere. Finally, the spring AO-related atmospheric circulation change contributes to spring SAT anomalies over the mid-high latitudes of the Eurasian continent via wind-induced temperature advection. The observed connection between autumn Arctic SIC and subsequent spring Eurasian SAT, as well as the spring AO-like atmospheric anomalies associated with the Arctic SIC is reproduced in the FGOALS-s2 simulations.

Furthermore, we have developed an empirical model to hindcast the Eurasian spring SAT via employing a combination of the spring AO index and preceding autumn Arctic SIC index. The results show that the cross validation correlation coefficients of the empirical model are much higher than those employing only the spring AO index to forecast the Eurasian spring SAT variation. This indicates that the autumn Arctic SIC, indeed could provide additional sources for the prediction of Eurasian spring SAT.

Impacts of the Arctic sea ice loss on climate anomalies over the mid-latitudes of the Northern Hemisphere have been substantially investigated in previous studies. Compared with previous studies, the new findings and implications of this study are as follows.

First, previous studies were mainly focused on analyzing influences of the preceding Arctic SIC change on the boreal winter SAT and related circulation anomalies. It is still unclear whether changes in the Arctic SIC may influence subsequent spring Eurasian SAT variations. It is noted that factors responsible for interannual variations of Eurasian SAT during boreal winter and spring are different (Gong et al. 2001; Wu and Wang 2002; Chen et al. 2016a). In addition, studies on the spring Eurasian SAT variations are much less than those on the winter SAT variations. This study analyzes impacts of the preceding Arctic sea ice change on the Eurasian SAT variation during boreal spring.

Second, most of previous studies identified significant impacts of the Arctic sea ice change in the Barents-Kara Sea on the climate anomalies over the mid-latitudes of the Northern Hemisphere. In comparison, our present study revealed that preceding autumn (September-October-averaged) Arctic sea ice variation in the Laptev Sea-eastern Siberian Sea-Beaufort Sea during preceding autumn has a significant connection with the following Eurasian spring SAT anomalies. The key regions identified in this study (Laptev Sea-Eastern Siberian Sea-Beaufort Sea) are generally different from those obtained in most of the previous studies (Barents-Kara Sea). This is attributed to the fact that large interannual variability of the Arctic SIC appears in the Laptev Sea-eastern Siberian Sea-Beaufort Sea (Barents-Kara Sea) during autumn (winter) (Figs. 2, 3 in the supplementary material; Yang et al. 2016).

Third, several previous studies have investigated the influence of the Arctic sea ice change on the subsequent AO variability (e.g., Jaiser et al. 2012; Liu et al. 2012a, b; Li and

Wu 2012; Nakamura et al. 2015; Yang et al. 2016). However, these studies mainly focused on analyzing the following winter AO. The detected Arctic SIC signal obtained in the present study for the spring AO variation is located differently from that obtained in the previous studies for the winter AO variation. For example, Jaiser et al. (2012) indicated that summer Arctic SIC change over the Siberian domain has a close connection with the following winter AO. Nakamura et al. (2015) suggested that increased (reduced) sea-ice area in November north of 65°N tends to result in more positive (negative) phases of the AO/NAO in the following winter. Yang et al. (2016) showed that Arctic SIC change in November over the Barents and Kara Seas has a close connection with the AO variability in the following February. By contrast, our present study emphasizes the role of Arctic SIC over the Laptev Sea-eastern Siberian Sea-Beaufort Sea in the early autumn (September-October-averaged) in influencing the subsequent spring AO variations. We have examined correlations of the Arctic SIC change over the Laptev Sea-eastern Siberian Sea-Beaufort Sea in the early autumn with the AO index in the following December, January, February and wintertime mean (DJF-averaged). The obtained correlation coefficients are weak and insignificant (not shown), indicating no obvious influences of the Arctic SIC over the Laptev Sea-eastern Siberian Sea-Beaufort Sea in the early autumn on the following winter AO variability. These are consistent with the results obtained in Fig. 10. Therefore, the above evidences imply that the regions with significant Arctic SIC signal for winter and spring AO variations are different. In addition, we have calculated the correlation coefficient between boreal winter AO index and spring AO index. The obtained correlation is weak and insignificant. This indicates that winter AO variability is independent of spring AO variability. Hence, it is necessary to study the Arctic SIC signals for the winter and spring AO variability separately. This study may provide an additional predictability source for the prediction of the spring AO.

Fourth, it is noted that spring AO has a significant impact on the East Asian summer monsoon activity and related precipitation anomalies over East Asia and western Pacific (Gong et al. 2011). Furthermore, several previous studies have demonstrated that spring AO is an important trigger for the outbreak of the subsequent winter ENSO events via modulating the westerly wind bursts over the tropical western Pacific (Nakamura et al. 2006, 2007; Chen et al. 2014a, 2016b). In particular, Chen et al. (2016b) reported that spring AO plays a key role in triggering the outbreak of the strong 2015–16 El Niño. These indicate that the findings in this paper may have several implications for better understanding the East Asian summer monsoon activity and ENSO events associated with the spring AO.

Note that, other factors, such as Eurasian snow cover, may also be important in relaying the influence the autumn

Arctic SIC on the subsequent spring Eurasian SAT. For example, studies found that snow cover extent (SCE) anomalies at October over Eurasia have a significant influence on the subsequent January AO via stratosphere-troposphere coupling process (e.g., Cohen et al. 2007, 2012). We have examined evolutions of the SCE anomalies from autumn to subsequent spring obtained by regression on the autumn Arctic SIC index (not shown). It shows that pronounced SCE anomalies are observed mainly over East Europe south of 60°N persisting from winter to spring. Whether these SCE anomalies have a contribution to the spring atmospheric circulation anomalies over the mid-high latitudes of Eurasia associated with the preceding autumn Arctic SIC remain to be explored.

**Acknowledgements** We thank two anonymous reviewers for their constructive suggestions and comments, which helped to improve the paper. This study is supported by the National Natural Science Foundation of China Grants (41530425, 41605050, 41475081, and 41661144016), the Young Elite Scientists Sponsorship Program by CAST, and the China Postdoctoral Science Foundation (2017T100102).

## References

- Ambaum MHP, Hoskins B (2002) The NAO troposphere-stratosphere connection. *J Clim* 15:1969–1978
- Andrews DG, Holton JR, Leovy CB (1987) *Middle atmosphere dynamics*. Academic Press, Dublin p 489
- Baldwin MP, Dunkerton TJ (1999) Downward propagation of the Arctic Oscillation from the stratosphere to the troposphere. *J Geophys Res* 104:30,937–946. <https://doi.org/10.1029/1999JD900445>
- Baldwin MP, Dunkerton TJ (2001) Stratospheric harbingers of anomalous weather regimes. *Science* 294:581–584. <https://doi.org/10.1126/science.1063315>
- Bao Q, Coauthors (2013) The flexible global ocean atmosphere-land system model, spectral version 2: FGOALS-s2. *Adv Atmos Sci* 30:561–576
- Beniston M (2004) The 2003 heat wave in Europe: a shape of things to come? An analysis based on Swiss climatological data and model simulations. *Geophys Res Lett* 31:L02202. <https://doi.org/10.1029/2003GL018857>
- Charney JG, Drazin G (1961) Propagation of planetary-scale disturbances from the lower into the upper atmosphere. *J Geophys Res* 66:83–109
- Chen W, Graf HF, Takahashi M (2002) Observed interannual oscillations of planetary wave forcing in the Northern Hemisphere winter. *Geophys Res Lett* 29:2073. <https://doi.org/10.1029/2002GL016062>
- Chen W, Takahashi M, Graf HF (2003) Interannual variations of stationary planetary wave activity in the northern winter troposphere and stratosphere and their relations to NAM and SST. *J Geophys Res* 108:4797. <https://doi.org/10.1029/2003JD003834>
- Chen S, Chen W, Wei K (2013) Recent trends in winter temperature extremes in eastern China and their relationship with the Arctic Oscillation and ENSO. *Adv Atmos Sci* 30:1712–1724. <https://doi.org/10.1007/s00376-013-2296-8>
- Chen S, Yu B, Chen W (2014a) An analysis on the physical process of the influence of AO on ENSO. *Clim Dyn* 42:973–989. <https://doi.org/10.1007/s00382-012-1654-z>
- Chen Z, Wu R, Chen W (2014b) Impacts of autumn Arctic sea ice concentration changes on the East Asian winter monsoon variability. *J Clim* 27:5433–5450. <https://doi.org/10.1175/JCLI-D-13-00731.1>
- Chen S, Wu R, Liu Y (2016a) Dominant modes of interannual variability in Eurasian surface air temperature during boreal spring. *J Clim* 29:1109–1125. <https://doi.org/10.1175/JCLI-D-15-0524.1>
- Chen S, Wu R, Chen W, Yu B, Cao X (2016b) Genesis of westerly wind bursts over the equatorial western Pacific during the onset of the strong 2015–2016 El Niño. *Atmos Sci Lett* 17:384–391
- Cheung H, Zhou W, Mok H, Wu M (2012) Relationship between Ural-Siberian Blocking and the East Asian winter monsoon in relation to the Arctic Oscillation and the El Niño-Southern Oscillation. *J Clim* 25:4242–4257. <https://doi.org/10.1175/JCLI-D-11-00225.1>
- Christiansen B (2001) Downward propagation of zonal mean zonal wind anomalies from the stratosphere to the troposphere: model and reanalysis. *J Geophys Res* 106(D21):307–322. <https://doi.org/10.1029/2000JD000214>
- Cohen JL, Barlow MA, Kushner PJ, Saito K (2007) Stratosphere-troposphere coupling and links with Eurasian land surface variability. *J Clim* 20(21):5335–5343
- Cohen JL, Furtado JC, Barlow MA, Alexeev VA, Cherry JE (2012) Arctic warming, increasing snow cover and widespread boreal winter cooling. *Environ Res Lett* 7(1):014007
- Collins WD, Coauthors (2006) The Community Climate System Model version 3 (CCSM3). *J Clim* 19:2122–2143
- Comiso JC, Parkinson CL, Gersten R, Stock L (2008) Accelerated decline in the Arctic sea ice cover. *Geophys Res Lett* 35:L01703. <https://doi.org/10.1029/2007GL031972>
- D'Arrigo R, Wilson R, Li J (2006) Increased Eurasian tropical temperature amplitude difference in recent centuries: implications for the Asian monsoon. *Geophys Res Lett* 33:L22706. <https://doi.org/10.1029/2006GL027507>
- Dee DP, and Coauthors (2011) The ERA-Interim reanalysis: configuration and performance of the data assimilation system. *Quart J Roy Meteor Soc* 137:553–597. <https://doi.org/10.1002/qj.828>
- Deser C, Tomas R, Alexander M, Lawrence D (2010) The seasonal atmospheric response to projected Arctic sea ice loss in the late twenty-first century. *J Clim* 23:333–351. <https://doi.org/10.1175/2009JCLI3053.1>
- Duchon CE (1979) Lanczos filtering in one and two Dimensions. *J Appl Meteorol* 18:1016–1022
- Edmon H, Hoskins BJ, McIntyre ME (1980) Eliassen-Palm cross sections for the troposphere. *J Atmos Sci* 37:2600–2616
- Francis JA, Vavrus SJ (2012) Evidence linking Arctic amplification to extreme weather in mid-latitudes. *Geophys Res Lett* 39:L06801. <https://doi.org/10.1029/2012GL051000>
- Francis JA, Chan W, Leathers DJ, Miller JR, Veron DE (2009) Winter Northern Hemisphere weather patterns remember summer Arctic sea-ice extent. *Geophys Res Lett* 36:L07503. <https://doi.org/10.1029/2009GL037274>
- Gao Y, Sun J, Li F, He S, Stein S, Yan Q, Zhang Z, Katja L, Noel K, Tore F, Suo L (2015) Arctic sea ice and Eurasian climate: a review. *Adv Atmos Sci* 32:92–114
- Gong DY, Wang SW, Zhu JH (2001) East Asian winter monsoon and Arctic oscillation. *Geophys Res Lett* 28:2073–2076. <https://doi.org/10.1029/2000GL012311>
- Gong DY, Yang J, Kim SJ, Gao YQ, Guo D, Zhou TJ, Hu M (2011) Spring Arctic Oscillation-East Asian summer monsoon connection through circulation changes over the western North Pacific. *Clim Dyn* 37:2199–2216
- Graf HF, Zanchettin D (2012) Central Pacific El Niño, the “subtropical bridge,” and Eurasian climate. *J Geophys Res* 117(D1):D01102. <https://doi.org/10.1029/2011JD016493>
- Ham YG, Kug JS, Park JY, Jin FF (2013) Sea surface temperature in the north tropical Atlantic as a trigger for El Niño/Southern Oscillation events. *Nat Geosci* 6:112–116

- Henderson-Sellers A (1996) Soil moisture: a critical focus for global change studies. *Glob Pl Chang* 13:3–9
- Holton JR (2004) An introduction to dynamic meteorology. 4, Academic Press, Dublin, 535
- Honda M, Inoue I, Yamane S (2009) Influence of low Arctic sea ice minima on anomalously cold Eurasian winters. *Geophys Res Lett* 36:L08707. <https://doi.org/10.1029/2008GL037079>
- Hopsch S, Cohen J, Dethloff K (2012) Analysis of a link between fall Arctic sea ice concentration and atmospheric patterns in the following winter. *Tellus* 64A:18624. <https://doi.org/10.3402/tellusa.v64i0.18624>
- Huang RH, Gambo K (1983) On the other wave guide of the quasi-stationary planetary waves in the Northern Hemisphere winter. *Sci China B* 26:940–950
- Hurrell JW, Van Loon H (1997) Decadal variations in climate associated with the North Atlantic Oscillation. *Climatic Change at High Elevation Sites*, Diaz HF, Beniston M, Bradley R (eds), Springer, Heidelberg 69–94
- Inoue J, Hori ME, Takaya K (2012) The role of Barents Sea ice in the wintertime cyclone track and emergence of a warm-Arctic cold-Siberian anomaly. *J Clim* 25:2561–2568. <https://doi.org/10.1175/JCLI-D-11-00449.1>
- Ionita M, Lohmann G, Rambu N, Scholz P (2012) Dominant modes of diurnal temperature range variability over Europe and their relationships with large-scale atmospheric circulation and sea surface temperature anomaly patterns. *J Geophys Res* 117:D15111. <https://doi.org/10.1029/2011JD016669>
- Jaiser R, Dethloff K, Handorf D, Rinke A, Cohen J (2012) Impact of sea ice cover changes on the Northern Hemisphere atmospheric winter circulation. *Tellus A* 64:11,595
- Kim HJ, Ahn JB (2012) Possible impact of the autumnal North Pacific SST and November AO on the East Asian winter temperature. *J Geophys Res* 117:D12104. <https://doi.org/10.1029/2012JD017527>
- Kim BM, Son SW, Min SK, Jeong JH, Kim SJ, Zhang Z, Shim T, Yoon JH (2014) Weakening of the stratospheric polar vortex by Arctic sea-ice loss. *Nat Commun* 5:4646
- King MP, Hell M, Keenlyside N (2016) Investigation of the atmospheric mechanisms related to the autumn sea ice and winter circulation link in the Northern Hemisphere. *Clim Dyn* 46:1185–1195. <https://doi.org/10.1007/s00382-015-2639-5>
- Kug JS, Jeong JH, Jang YS, Kim BM, Folland CK, Min SK, Son SW (2015) Two distinct influences of Arctic warming on cold winters over North America and East Asia. *Nat Geosci* 8:759–762. <https://doi.org/10.1038/ngeo2517>
- Li F, Wang HJ (2013) Relationship between Bering Sea ice cover and East Asian winter monsoon year-to-year variations. *Adv Atmos Sci* 30:48–56. <https://doi.org/10.1007/s00376-012-2071-2>
- Li JP, Wu ZW (2012) Importance of autumn Arctic sea ice to northern winter snowfall. *Proc Natl Acad Sci USA* 109:E1898. <https://doi.org/10.1073/pnas.1205075109>
- Lin PF, Yu YQ, Liu HL (2013) Long-term stability and oceanic mean state simulated by the coupled model FGOALS-s2. *Adv Atmos Sci* 30:175–192
- Liu X, Yanai M (2001) Relationship between the Indian monsoon rainfall and the tropospheric temperature over the Eurasian continent. *Quart J Roy Meteor Soc* 127:909–937. <https://doi.org/10.1002/qj.49712757311>
- Liu HL, Lin PF, Yu YQ, Zhang X (2012a) The baseline evaluation of LASG/IAP Climate system Ocean Model (LICOM) version 2.0. *J Meteorol Res* 26:318–329
- Liu JP, Curry JA, Wang HJ, Song MR, Horton RM (2012b) Impact of declining Arctic sea ice on winter snowfall. *Proc Natl Acad Sci USA* 109:4074–4079. <https://doi.org/10.1073/pnas.1114910109>
- Matsuura K, Willmott CJ (2009) Terrestrial air temperature: 1900–2008 gridded monthly time series (version 4.01), University of Delaware Dept. of Geography Center. (Available at [http://www.esrl.noaa.gov/psd/data/gridded/data.UDeI\\_AirT\\_Precip.html](http://www.esrl.noaa.gov/psd/data/gridded/data.UDeI_AirT_Precip.html)). Accessed 6 Aug 2015
- McCusker KE, Fyfe JC, Sigmond M (2016) Twenty-five winters of unexpected Eurasian cooling unlikely due to Arctic sea-ice loss. *Nat Geosci* 9:838–842
- Miyazaki C, Yasunari T (2008) Dominant interannual and decadal variability of winter surface air temperature over Asia and the surrounding oceans. *J Clim* 21:1371–1386. <https://doi.org/10.1175/2007JCLI1845.1>
- Mohanakumar K (2008) Stratosphere troposphere interactions. Springer, Heidelberg 416
- Nakamura T, Tachibana Y, Honda M, Yamane S (2006) Influence of the Northern Hemisphere annular mode on ENSO by modulating westerly wind bursts. *Geophys Res Lett* 33:L07709
- Nakamura T, Tachibana Y, Shimoda H (2007) Importance of cold and dry surges in substantiating the NAM and ENSO relationship. *Geophys Res Lett* 34:L22703
- Nakamura T, Yamazaki K, Iwamoto K, Honda M, Miyoshi Y, Ogawa Y, Ukita J (2015) A negative phase shift of the winter AO/NAO due to the recent Arctic sea-ice reduction in late autumn. *J Geophys Res* 120:3209–3227. <https://doi.org/10.1002/2014JD022848>
- North GR, Moeng FJ, Bell TL, Cahalan RF (1982a) The latitude dependence of the variance of zonally averaged quantities. *Mon Wea Rev* 110:319–326
- North GR, Bell TL, Cahalan RF, Moeng FJ (1982b) Sampling errors in the estimation of empirical orthogonal functions. *Mon Wea Rev* 110:699–706
- Ogi M, Tachibana Y, Yamazaki K (2003) Impact of the wintertime North Atlantic Oscillation (NAO) on the summertime atmospheric circulation. *Geophys Res Lett* 30:1704. <https://doi.org/10.1029/2003GL017280>
- Oleson KW et al (2004) Technical description of the Community Land Model (CLM), NCAR Technical Note, NCAR/TN-461 + STR, p. 173. <https://doi.org/10.5065/D6N877R0>
- Peng G, Meier WN, Scott DJ, Savoie MH (2013) A long-term and reproducible passive microwave sea ice concentration data record for climate studies and monitoring. *Earth Syst Sci Data* 5(2):311–318. <https://doi.org/10.5194/essd-5-311-2013>
- Perlwitz J, Harnik N (2003) Observational evidence of a stratospheric influence on the troposphere by planetary wave reflection. *J Clim* 16:3011–3026
- Petoukhov V, Semenov V (2010) A link between reduced Barents–Kara sea ice and cold winter extremes over northern continents. *J Geophys Res* 115:D21111. <https://doi.org/10.1029/2009JD013568>
- Plumb RA (1985) On the three-dimensional propagation of stationary waves. *J Atmos Sci* 42:217–229
- Polvani LM, Waugh DW (2004) Upward wave activity flux as a precursor to extreme stratospheric events and subsequent anomalous surface weather regimes. *J Climate* 17:3548–3554
- Rayner NA, Parker DE, Horton EB, Folland CK, Alexander LV, Rowell DP, Kent EC, Kaplan A (2003) Global analyses of sea surface temperature, sea ice, and night marine air temperature since the late nineteenth century. *J Geophys Res* 108:4407. <https://doi.org/10.1029/2002JD002670>
- Screen JA, Simmonds I (2010) The central role of diminishing sea ice in recent Arctic temperature amplification. *Nature* 464:1334–1337. <https://doi.org/10.1038/nature09051>
- Serreze MC, Holland MM, Stroeve J (2007) Perspectives on the Arctic's shrinking sea ice cover. *Science* 315:1533–1536. <https://doi.org/10.1126/science.1139426>
- Simpson IR, Blackburn M, Haigh JD (2009) The role of eddies in driving the tropospheric response to stratospheric heating perturbations. *J Atmos Sci* 66(5):1347–1365. <https://doi.org/10.1175/2008JAS2758.1>
- Song Y, Robinson W (2004) Dynamical mechanisms for stratospheric influences on the troposphere. *J Atmos Sci* 61(14):1711–1725

- Stott PA, Stone DA, Allen MR (2004) Human contribution to the European heatwave of 2003. *Nature* 432:610–614. <https://doi.org/10.1038/nature03089>
- Sun YT, Wang SY, Yang YQ (1983) Studies on cool summer and crop yield in northeast China (in Chinese). *Acta Meteor Sin* 41:313–321
- Sun JQ, Wang HJ, Yuan W (2008) Decadal variations of the relationship between the summer North Atlantic Oscillation and middle East Asian air temperature. *J Geophys Res* 113:D15107. <https://doi.org/10.1029/2007JD009626>
- Sun L, Perlwitz J, Hoerling M (2016a) What caused the recent “Warm Arctic, Cold Continents” trend pattern in winter temperatures? *Geophys Res Lett*. <https://doi.org/10.1002/2016GL069024>
- Sun C, Yang S, Li WJ, Zhang R, Wu R R (2016b) Interannual variations of the dominant modes of East Asian winter monsoon and possible links to Arctic sea ice. *Clim Dyn* 47:481–491
- Tang Q, Zhang X, Yang X, Francis JA (2013) Cold winter extremes in northern continents linked to Arctic sea ice loss. *Environ Res Lett* 8:014036
- Thompson DW, Wallace JM (1998) The Arctic Oscillation signature in the wintertime geopotential height and temperature fields. *Geophys Res Lett* 25:1297–1300. <https://doi.org/10.1029/98GL00950>
- Vallis G (2006) Atmospheric and oceanic fluid dynamics: fundamentals and large-scale circulation. Cambridge University Press, Cambridge, p 745
- Vihma T (2014) Effects of Arctic sea ice decline on weather and climate: a review. *Surv Geophys* 35:1175–1214. <https://doi.org/10.1007/s10712-014-9284-0>
- Wang L, Chen W (2010) Downward Arctic Oscillation signal associated with moderate weak stratospheric polar vortex and the cold December 2009. *Geophys Res Lett* 37:L09707. <https://doi.org/10.1029/2010GL042659>
- Webster PJ, Yang S (1992) Monsoon and ENSO: selectively interactive systems. *Quart J Roy Meteor Soc* 118:877–926. <https://doi.org/10.1002/qj.49711850705>
- Wu R, Chen S (2016) Regional change in snow water equivalent–surface air temperature relationship over Eurasia during boreal spring. *Climate Dyn* 47:2425–2442. <https://doi.org/10.1007/s00382-015-2972-8>
- Wu BY, Wang J (2002) Winter Arctic oscillation, Siberian high and East Asian winter monsoon. *Geophys Res Lett* 29:1897. <https://doi.org/10.1029/2002GL015373>
- Wu R, Yang S, Liu S, Sun L, Lian Y, Gao ZT (2010) Changes in the relationship between Northeast China summer temperature and ENSO. *J Geophys Res* 115:D21107. <https://doi.org/10.1029/2010JD014422>
- Wu R, Yang S, Liu S, Sun L, Lian Y, Gao Z (2011a) Northeast China summer temperature and North Atlantic SST. *J Geophys Res* 116:D16116. <https://doi.org/10.1029/2011JD015779>
- Wu BY, Su JZ, Zhang RH (2011b) Effects of autumn–winter Arctic sea ice on winter Siberian High. *Chin Sci Bull* 56:3220–3228. <https://doi.org/10.1007/s11434-011-4696-4>
- Wu BY, Overland JE, D’Arrigo R (2012) Anomalous Arctic surface wind patterns and their impacts on September sea ice minima and trend. *Tellus* 64:18590. <https://doi.org/10.3402/tellusa.v64i0.18590>
- Wu R, Zhao P, Liu G (2014) Change in the contribution of spring snow cover and remote oceans to summer air temperature anomaly over Northeast China around 1990. *J Geophys Res* 119:663–676
- Wu ZW, Li XX, Li YJ, Li Y (2016) Potential influence of Arctic sea ice to the interannual variations of East Asian spring precipitation. *J Clim* 29:2797–2813
- Yang X, Yuan X, Ting M (2016) Dynamical link between the Barents–Kara sea ice and the Arctic Oscillation. *J Clim* 29:5103–5122
- Yao PZ (1995) The climate features of summer low temperature cold damage in northeast China during recent 40 years (in Chinese). *J Catastrophol* 10:51–56
- Ye K, Wu R, Liu Y (2015) Interdecadal change of Eurasian snow, surface temperature, and atmospheric circulation in the late 1980s. *J Geophys Res* 120:2738–2753. <https://doi.org/10.1002/2015JD023148>
- Zuo J, Ren HL, Wu BY, Li WJ (2016) Predictability of winter temperature in China from previous autumn Arctic sea ice. *Clim Dyn* 47:2331–2343
- Zveryaev II, Gulev SK (2009) Seasonality in secular changes and interannual variability of European air temperature during the twentieth century. *J Geophys Res* 114:D02110. <https://doi.org/10.1029/2008JD010624>